Ruthenium Nanoparticles for Catalytic Water Splitting

Jordi Creus, Jonathan De tovar, Nuria Romero, Jordi García-antón, Karine Philippot, Roger Bofill, Xavier Sala

Ruthenium Nanoparticles for Catalytic Water Splitting

Jordi Creus+,[a,b,c] Jonathan De Tovar+,[a] Nuria Romero,[a] Jordi García-Antón,[a] Karine Philippot*,[b,c] Roger Bofill*,[a] and Xavier Sala*,[a]

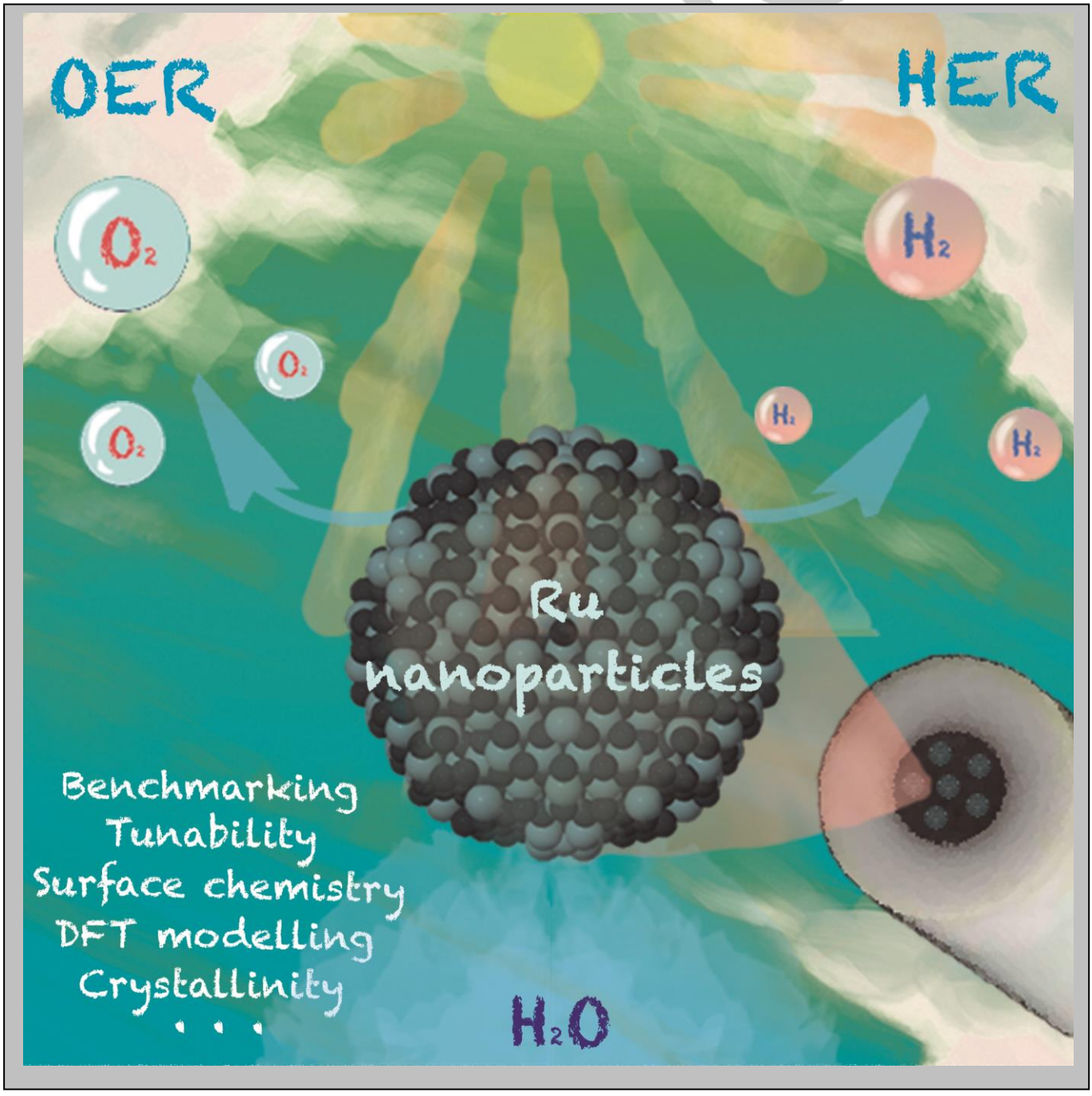

Abstract: Both global warming and the limited fossil resources make the transition from fossil to solar fuels an urgent matter. In this regard, the splitting of water activated by sunlight is a sustainable and carbon-free new energy conversion scheme able to produce efficient technological devices. Having at disposal appropriate catalysts is essential for the proper kinetics of the two key processes involved, namely the oxygen evolution reaction (OER) and the hydrogen evolution reaction (HER). During the last decade nanoparticulated Ru derivatives have emerged as true potential substitutes for the state-of-the art Pt and IrOx species for HER and OER, respectively. Thus, after a first section summarizing the most common methods for catalyst benchmarking, this review covers the most significant developments on Ru-based nanoparticles used as catalysts for the water splitting process. Furthermore, the key factors that govern the catalytic performance of these nanocatalysts are discussed in view of future research directions.

1. Introduction

High consumption of fossil fuels together with the accumulation of CO_2 in the atmosphere due to their combustion have put forward the urgent need for a cheap, clean and carbon-neutral energy source. One of the most attractive and possible solutions to face this challenge is the production of H_2 by the splitting of water (WS, Eq. 1) photo-activated by sunlight. This method to produce H_2 mimics what green plants, algae and cyanobacteria do to store sunlight energy in chemical bonds, and is one of the processes known as artificial photosynthesis.[1] In this redox process, water is oxidized to molecular oxygen at the anode (Eq. 2a and 2b at neutral/acidic and basic pH, respectively) and the released electrons and protons produce molecular hydrogen at the cathode (Eq. 3a and 3b at neutral/acidic and basic pH, respectively).

$$2\,H_2O \rightarrow O_2 + 2\,H_2 \qquad \text{Eq. 1}$$

$$2\,H_2O \rightarrow O_2 + 4\,H^+ + 4\,e^- \qquad \text{Eq. 2a}$$
$$4\,OH^- \rightarrow O_2 + 2\,H_2O + 4\,e^- \qquad \text{Eq. 2b}$$

$$4\,H^+ + 4\,e^- \rightarrow 2\,H_2 \qquad \text{Eq. 3a}$$
$$4\,H_2O + 4\,e^- \rightarrow 2\,H_2 + 4\,OH^- \qquad \text{Eq. 3b}$$

[a] Dr. J. Creus+, Dr. J. De Tovar+, Dr. N. Romero, Dr. J. García-Antón, Dr. R. Bofill*, Dr. X. Sala*
Departament de Química, Facultat de Ciències
Universitat Autònoma de Barcelona
08193 Bellaterra, Catalonia (Spain)
E-mail: Roger.Bofill@uab.cat; Xavier.Sala@uab.cat
[b] Dr. J. Creus+, Dr. K. Philippot*
Laboratoire de Chimie de Coordination du CNRS
205 route de Narbonne, F-31077, Toulouse Cédex 04 (France)
E-mail: Karine.Philippot@lcc-toulouse.fr
[c] Dr. J. Creus+, Dr. K. Philippot*
Université de Toulouse, UPS, INPT, LCC,
F-31077 Toulouse Cédex 04 (France)
[+] Both authors contributed equally to this work.

These processes are kinetically slow because of their mechanistic complexity -especially for the oxidation half reaction- and the difficulty of evolving gases from a liquid phase, and therefore it is of upmost importance to find proper catalytic systems able to accelerate them. In this context, nanoparticles (NPs) are highly interesting chemical systems owing to their unusual properties at the interface of those of molecular species and bulk counterparts.[2] NPs, if properly characterized,[3] are of particular interest for applications in catalysis given their high specific surface area and the possibility of depositing/embedding them in various supports and also to surface-functionalize them through diverse strategies. This offers great opportunities in terms of reusability, for example in electrocatalytic processes in which they can act as the active supported species onto solid electrodes.

Concerning the oxygen evolution reaction (OER, Eq. 2a/2b), anodes made with iridium oxide (IrO_x) have been historically used to perform this first half-reaction of the water splitting process, since this material shows excellent electrocatalytic performance under the harsh conditions required.[4] However, significant activity of heterogeneous RuO_2 in the OER has also been known for 30 years,[5,6] which is attributed to the average binding energy of the surface bonded oxygen species.[7] In fact, several interesting features make RuO_2 particularly promising to replace the highly active state-of-the-art IrO_x species, which are expensive and scarce, in proton exchange membrane (PEM) electrolyzers for WS. Contrarily to traditional water electrolyzers that operate in basic media, PEM WS systems work under acidic conditions and provide numerous performance advantages that make them ideal devices for the delocalized storage of renewable electricity at a small scale.[8] Given that active and stable 1st row transition metal-based oxide catalysts for the OER in acidic media are elusive, RuO_2 turns out to be a remarkable candidate for PEM systems, especially if taking into account that Ru is at least six times cheaper than Ir. However, for RuO_2 to be employed for practical applications, maximizing the number of active sites at its surface is of paramount importance in order to increase its efficiency. Therefore, nanoparticulated systems, with large surface area to volume ratios, present obvious advantages and are particularly desirable.

Today most of the mechanistic knowledge available on the OER comes from the research performed for the last 40 years on Ru molecular complexes.[9] Cycling even at the millisecond timescale,[10] Ru complexes have proven to be highly active electrocatalysts for the OER, showing remarkable stability if properly designed.[11] But the reaction rates of their heterogeneous counterparts, namely RuO_2, are typically several orders of magnitude lower, even when nanoparticulated materials are employed; turnover frequency (TOF) values are below 1 s^{-1} (see Section 3 below), that highly contrasts to TOFs in the 10000 s^{-1} range for the best Ru molecular OER catalysts.[10] However, a drawback frequently threatens the catalytic performance of Ru molecular water oxidation catalysts (WOCs): they can be vulnerable under the highly oxidizing conditions used and show a tendency towards ligand oxidation/substitution and thus metal oxide formation, among

other processes.[11] Interestingly, the *in situ* formation of RuO_2 from the decomposition of grafted Ru molecular complexes under catalytic turnover conditions has recently led to both dramatically increased activities and stabilities.[12] Thus, unraveling the factors ruling the performance of RuO_2 OER catalysts, namely under the form of NPs, is of upmost relevance. The attention of the scientific community towards this subject has increased in recent years.

The second half-reaction of water splitting, the hydrogen evolution reaction (HER, Eq. 3a), is mechanistically simpler than the OER at acidic/neutral pH (Eq. 2a). Compared to the oxidative process where four H-O bonds have to be broken and an O=O double bond formed while releasing 4 electrons and 4 protons, the HER involves only the formation of one H-H bond by the reduction of two H^+ groups. This divergence is evidenced with the onset overpotential (η_0) -the difference between the thermodynamic equilibrium potential and the actual potential where the catalytic reaction starts- that heterogeneous catalysts require for each half-reaction, in general being < 100 mV for HER electrocatalysts and > 200 mV for OER electrocatalysts (Tables 1-4).

In the solid phase, Pt has been the most used metal for the HER, being the most active metal in reducing protons, especially at acidic pH values. In these conditions, the M-H bond energy plays a key role in proton reduction catalysis given that a high M-H binding energy eases the adsorption of protons (but hardens the H_2 desorption), whereas a low M-H binding energy has an opposite effect. Platinum is located at the centre of the so-called volcano plot for proton reduction catalysts because it possesses the optimum M-H binding energy, which is neither too low nor too high.[13,14] Ruthenium presents a M-H bond only slightly weaker compared to Pt, which hardly decreases the HER catalytic efficiency, both according to experimental results and DFT calculations.[15] Furthermore, Ru has been shown to be stable both under acidic and basic conditions which provides this metal an extreme versatility in terms of working conditions, in contrast to Pt, whose long-term stability at basic pH is not optimal.[16] Additionally, the cost of Ru is noticeably lower -at least six times- than that of Pt. These characteristics all together have boosted the re-birth of Ru metal as a HER electrocatalyst in the last five years, particularly when it is in the form of NPs.

This review focuses on the most remarkable Ru-based NP systems reported as HER/OER (electro)catalysts for the water splitting process and highlights the key factors that rule the catalytic performance of these nanomaterials. Given the crucial role of benchmarking for the objective assessment of the reported systems, a forefront section dedicated to this end has been included. Finally, future research directions are also discussed.

Dr. Jordi Creus graduated in Chemistry at the Universitat Autònoma de Barcelona (UAB) and obtained an M. Sc. Diploma in "Synthesis, catalysis and molecular design" in 2014 by the Rovira i Virgili University (URV) and the Catalan Institute of Chemical Research (ICIQ) in Tarragona. In 2018 he completed his PhD in Chemistry in an international joint supervision between the UAB and the Laboratoire de Chimie de Coordination (LCC-CNRS) at the Paul Sabatier University (UPS) in Toulouse.

Dr. Jonathan De Tovar obtained his PhD in Pd and Co-based (nano)catalysts for C-C coupling and artificial photosynthesis from the Universitat Autònoma de Barcelona (UAB) in 2018. By the beginning of 2019, he joined Prof. Laurent Djakovitch group at the Institut de recherches sur la catalyse et l'environnement de Lyon (IRCELYON) as postdoctoral researcher, where he works on the development of hyperactive catalytic species in the liquid phase from molecular or colloidal systems.

Dr. Nuria Romero, born in Toledo (Spain), is a postdoctoral fellow and teacher at the Universitat Autònoma of Barcelona (Spain). She graduated from Chemistry at the Universidad de Castilla-La Mancha (Spain) in 2011. She concluded the PhD in organometallic chemistry at the Laboratoire de Chimie de Coordination of Toulouse (France) in 2014. Then she did an 18 months postdoctoral stay for the development of new catalysts for olefin polymerization at the Université de Rennes 1 (France), in collaboration with Total Raffinage Chimie in Feluy (Belgium). Since 2016 she has focused in the development of new catalysts and nanocatalysts for the water splitting reaction.

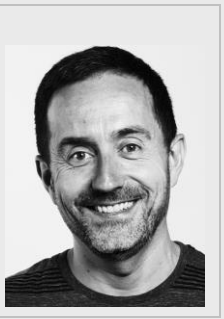

Dr. Jordi García-Antón was born in Cubelles (Barcelona, Spain) in 1976. He received his PhD in Chemistry in 2003 from the Universitat Autònoma de Barcelona (UAB). After a postdoctoral stay at the Laboratoire de Chimie de Coordination in Toulouse (France) in the group of Dr. Bruno Chaudret, he joined the UAB as a lecturer in chemistry. His research interest is focused on coordination chemistry on the surface of metallic nanoparticles and artificial photosynthesis.

Dr. Karine Philippot. After a PhD in Chemistry at the University of Toulouse and a postdoctoral position at Catalysis Department of Rhodia-Lyon, Karine Philippot integrated the CNRS Laboratory of Coordination Chemistry in Toulouse (France) where she is Senior Researcher and the head of team "Engineering of Metal Nanoparticles". Her research concerns metal nanoparticles and composite nanomaterials synthesis by using molecular chemistry concepts. The domains of application are colloidal and supported catalysis as well as energy. She is co-author of >170 peer reviewed papers (including 5 reviews, 13 proceedings, 9 book chapters, 6 patents) and co-editor of the book "*Nanomaterials in Catalysis*" (Wiley).

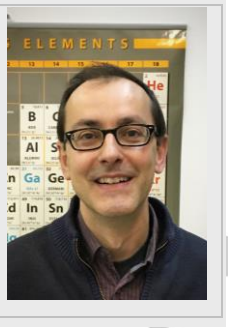

Dr. Roger Bofill obtained the PhD in Chemistry at the Universitat Autònoma de Barcelona (UAB) in 2001. After a postdoctoral stay in Prof. M.S. Searle group at the Centre for Biomolecular Sciences, University of Nottingham (UK), he rejoined the UAB as a lecturer and researcher in 2004, obtaining his tenure in 2009. His recent research interests have focused on the use of chemistry as a tool for understanding the complexity of our biological world and obtaining a source of sustainable energy.

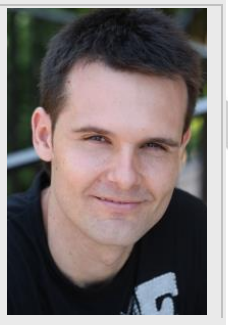

Dr. Xavier Sala obtained his PhD in Chemistry from the University of Girona (UdG) in 2007. After postdoctoral research with P. W. N. M. van Leeuwen and A. Llobet at ICIQ, he is currently Associate Professor of Chemistry at the Universitat Autònoma de Barcelona (UAB) where he leads the Selective Oxidation Catalysis (SelOxCat) research group. His research interest focuses on the study, comprehension and development of the key reactions involved in the production of renewable fuels through redox catalysis.

2. General methodology and activity benchmarking

The majority of Ru-based NP systems described as HER/OER catalysts have been evaluated electrochemically after deposition onto the surface of conducting electrodes, with glassy carbon (GC) electrodes being the most common example. However, the use of pressed Pt powder discs as alternative to oxidizable C-based electrodes has also been reported for OER applications.[17,18] Since in both HER and OER gases are continuously evolving, the use of glassy carbon rotating disk electrodes (RDE-GC) is highly recommended. The disk rotation results in a laminar flow of solution towards and across the electrode that controls the steady-state current in spite of diffusion. At the same time this minimizes the H_2 or O_2 gas accumulation at the electrode surface, thus ensuring a better accessibility of the catalyst active sites under turnover conditions and also a more real quantification of evolved gas when analyzed with specific probes.

Meaningful comparison of the performance and stability of electrocatalytic materials prepared for the WS reactions presents inherent difficulties arising from the wide set of conditions (varied supports and catalyst loadings, diverse electrolytes and pH ranges,…) employed to test their performance. Traditionally, the electrochemical activity of heterogeneous catalysts has been normalized by the total amount of catalyst or metal present, thus yielding the so-called mass activity parameter (generally expressed as $A \cdot mg^{-1}$ or $A \cdot g^{-1}$).[8,19] However, this represents an average activity that does not take into account the putative presence of different sites in the sample (e.g. exposed/active sites vs. unexposed/inactive sites). Thus, several authors have proposed several methodologies for normalizing the vast electrochemical data available for both HER and OER catalysis.[4,16,19,20,21,22,23] Therefore, a set of benchmarking parameters are nowadays used to assess the intrinsic activity and stability of the systems in a relatively fast and easy/affordable manner. An overview of the parameters typically defined to this purpose and the most frequently related methodologies can be found hereafter.

The first relevant figure of merit is the overpotential at the beginning of the catalytic process, η_0, which can be distinguished by a change on the current intensity (i) due to a Faradaic process when performing voltammetric measurements. Accurately determining a slope change in a voltammetric experiment is not always straightforward and thus η_0 determination is typically not absent of subjectivity. Thus, the overpotential required to achieve a current density ($|j|$) of 10 $mA \cdot cm^{-2}$ (η_{10}), which is approximately the current density expected for a solar water-splitting device subjected to 1 sun illumination and working at a solar-to-fuel efficiency of 10%, has arisen as a commonly accepted benchmarking parameter for both HER and OER. In addition, in order to assess the stability of the studied catalysts, η_{10} can be compared at the beginning and after continuous catalytic turnover. Typical reaction times of 2 h are applied for short-term and more than 12 h for long-term stability tests, as proposed by Jaramillo *et al.*[16] It is noteworthy that long-term (> 12 h) stability tests are not frequently reported.

If the chosen benchmarking parameter is η_{10}, determining the active surface area of the tested electrocatalyst is of paramount importance in order to assess its activity. Note that η_{10} can also be (and is widely) measured by normalizing the obtained current intensities by the total geometric area of the employed electrode instead of that of the electrocatalyst. However, this methodology provides scarce information about the intrinsic activity of the catalyst, being of relatively low interest as a tool of objective benchmarking. Specific surface areas are commonly determined either by the so-called Brunauer–Emmett–Teller (BET) method,

which is based on gas adsorption measurements, or through electrochemical measurements. In general, BET is a well-defined empirical measurement leading to relatively accurate values of the *total* specific surface of the analyzed electrocatalyst. But given that not all surface sites are usually active, overestimation of the catalytically active surface area is common with this method, which leads to the underestimation of the intrinsic activity of the real active sites.[20] The electrochemical method to assess electrocatalyst surface areas relies on the determination of the *electrochemically active* surface area (ECSA). To determine the ECSA, it is necessary to measure the double-layer capacitance (C_{DL}) of the material, which can be assessed through two different methods. The first one, proposed by Jaramillo *et al.,* consists in the measurement of CVs at different scan rates in non-faradaic regions.[4,16,20] The second one is based on electrochemical impedance spectroscopy (EIS) measurements in the same non-faradaic regions. Although in general the C_{DL} measured by both methods tend to agree within ± 15%, some authors claim that the latter may be preferable.[19] From the ECSA values, the so-called roughness factor (RF) can be measured as RF = ECSA/geometrical electrode area. If the current density $|j|$ is normalized by the RF, the so-called specific activity ($|j_s|=|j|/RF$) can be obtained. It allows comparing the performance of very diverse systems with different catalyst loadings and electrode areas. Nevertheless, even if in principle the ECSA method is more realistic in terms of describing active surface sites, it shows important experimental difficulties that make it inaccurate, thus potentially leading either to the underestimation or overestimation of the true catalytically active area.[20] ECSA and BET were recently compared by Jaramillo and co-workers as methods for normalizing the activity of OER nanoparticulate electrocatalysts.[20] However, it remains unclear which should be the method of choice since it strongly depends on the type of solid to be studied. Thus, reporting specific activities per duplicate through both ECSA and BET seems a desirable practice to get higher confident results.

The determination of the turnover number (TON) and turnover frequency (TOF) per real catalytic active site is another significant benchmarking parameter to be discussed. Normally, the total number of active sites present in a metal-based catalyst deposited onto the surface of a conductive electrode can be directly determined by integrating the area below the CV oxidation or reduction peak according to Faraday's law, as is the case for Ni and Co-based nanocatalysts.[19] However, for the particular case of Ru-based NPs no redox processes are commonly observed except from the catalytic current. An alternative method can be used to determine the total number of metallic Ru active sites (which is also valid for metallic Pt). It is the so-called Cu Under-Potential Deposition method (UPD, Figure 1), in which all metallic Ru (or Pt) active sites are initially saturated with Cu atoms by selective Cu^{2+} electro-reduction (Figure 1a-b). Then, after a controlled oxidation (Figure 1c), deposited Cu atoms are released into the solution. Copper atoms can be quantified by the integration of the Cu oxidation wave area (Figure 1d), thus allowing to estimate the number of accessible metallic Ru (or Pt) active sites in the original system.[22,24] Once the total number of active sites present is known, the total amount of H_2 or O_2 gas molecules detected by a selective probe or the amount of evolved gas per time lapse can be normalized by the total quantity of active sites, thus leading to the TON and TOF values per real active site, respectively. The UPD method is particularly relevant for the benchmarking of HER electrocatalysts (see Section 4 below) where metallic Ru sites are the most common catalytically active species.

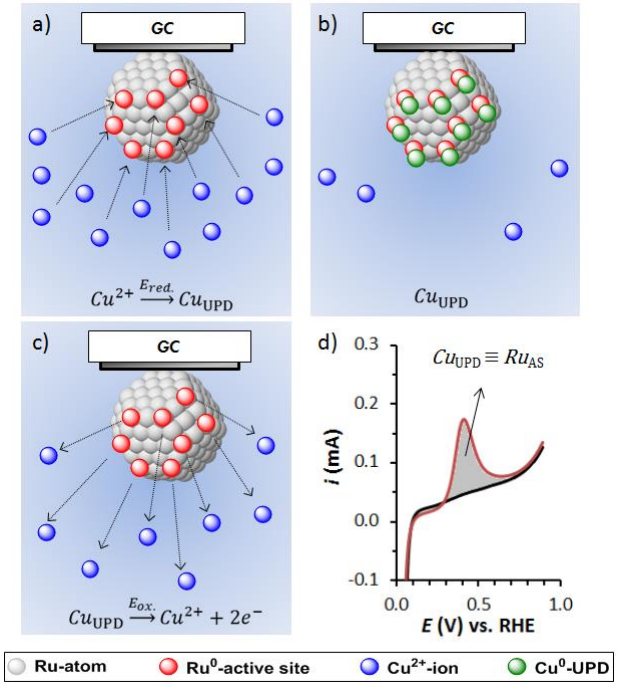

Figure 1. Schematic representation of the Cu Underpotential Deposition (UPD) method for the determination of catalytic metallic Ru active sites in Ru-based NPs.

Electrochemical Tafel plots, which are defined as the plot of log $|j|$ vs. η, constitute useful graphical tools for comparing the performance of electrocatalytic materials studied under analogous conditions and thus are suitable for benchmarking purposes.[25,26] Tafel plots can be extracted either from voltammograms, chronoamperometries/chronopotentiometries or from EIS measurements. The Tafel plot slope, expressed as $mV \cdot dec^{-1}$, gives information about the kinetics of the electrochemical process. Furthermore, in the particular case of HER, Tafel plots help inferring details on the mechanistic pathway of the catalytic act and, beyond, to classify the catalysts.[19] Thus, heterogeneous HER has been described to occur through two different reaction pathways, namely Volmer-Heyrovsky or Volmer-Tafel (Eqs. 4&5 and 4&6, respectively):[25,27]

Volmer: $Cat_{(s)} + H^+_{(aq)} + e^- \rightarrow Cat - H_{(ad)}$ Eq. 4

Heyrovsky: $Cat - H_{(ad)} + H^+_{(aq)} + e^- \rightarrow H_{2(s)} + Cat_{(s)}$ Eq. 5

Tafel: $2\ Cat - H_{(ad)} \rightarrow H_{2(s)} + 2\ Cat_{(s)}$ Eq. 6

The Volmer step (Eq. 4) is the adsorption of one proton onto the catalyst surface, and is common for all HER electrocatalysts. It is considered as a Proton Coupled Electron Transfer (PCET) step at the surface of the catalyst, and is alternatively called discharge reaction. The desorption step can either go through the electrodesorption of the adsorbed hydrogen atom with a H^+ in solution (Heyrovsky step, Eq. 5), which is also a PCET process, or through the recombination of two metal-hydride groups (M-H) from a unique nanoparticle or from two different ones (Tafel step, Eq. 6).

Thermodynamically, electrocatalysts are ruled by the Nernst equation, which allows to calculate the thermodynamic potentials as $E^0(H^+/H_2)$ = 0.00 - 0.05916 · pH. However, an overpotential (η) is always present, and the whole HER kinetics follow the Butler-Volmer equation[28] (Eq. 7),

$$|j| = |j_0|[-e^{-\frac{\alpha n F \eta}{RT}} + e^{(1-\alpha)\frac{nF\eta}{RT}}] \quad \text{Eq. 7}$$

where $|j|$ is the current density, $|j_0|$ is the exchange current density, i.e., the residual current of the catalytic system under non-faradaic conditions, α is the charge transfer coefficient, n is the number of electrons transferred, F is the Faraday constant, R is the ideal gas constant and T is the temperature. If $\eta >>$ RT/F, a linear relationship appears between η and log($|j|$) (Eqs. 8 and 9).

$$\eta = a + b \cdot log(|j|) = -\left(\frac{2.3RT}{\alpha nF}\right)\log(|j_0|) + \left(\frac{2.3RT}{\alpha nF}\right) \cdot \log(|j|) \quad \text{Eq. 8}$$

$$b = \frac{2.3RT}{\alpha nF} \quad \text{Eq. 9}$$

The slope (b, Eq. 9) of the Tafel plot (Eq. 8) gives kinetic information on the rate determining step (rds) among the different reaction pathways. In the case of HER, the rds depends on the binding energy of the M-H bond. Thus, if the rds of the reaction is the Volmer step, a typical Tafel slope of ≈ 120 mV·dec^{-1} is obtained. However, if the rds is the Heyrovsky or the Tafel step, characteristic slopes of ≈ 40 mV·dec^{-1} or ≈ 30 mV·dec^{-1} are observed, respectively.

In the case of OER, its higher mechanistic complexity makes the interpretation of Tafel plots more difficult. From a theoretical point of view, b can change from 120 mV·dec^{-1} to 30 and even 21 mV·dec^{-1} depending on the rds and the applied potential (the slope increases with increasing potentials).[25] Furthermore, apart from theoretical complications, important experimental drawbacks have been also reported.[23] First, the dependence of the Tafel slope with the manner in which a metal oxide has been prepared (*e.g.* the surface roughness) and the history of the electrode. Second, two distinct linear regions with different slopes can be recorded depending on the applied potential, which can be either due to a change of the rds within a given pathway or due to the influence of changing potential on the adsorption of reaction intermediates. And third, an increase of the slope with applied potential may not necessarily be mechanistically relevant but instead due to a reduction in the effective electrode surface area with increasing gas evolution at higher potentials. Altogether these may be the reasons why very rarely mechanistic conclusions are extracted from Tafel plot analysis of OER catalysts.

Finally, the selectivity of the catalysts is commonly measured through the Faradaic efficiency determination in a bulk electrolysis experiment. It corresponds to the percentage of the total amount of electrons that have circulated through the electrochemical system and were effectively used for evolving gas, according to Faraday's law. Also, when rotating ring disk electrodes (RRDE) are employed, the Faradaic efficiency of a HER/OER process can be directly determined from electrochemical measurements, without need of using selective gas detection probes.[19]

The benchmarking parameters that have been described here above will be used when available in the following sections of this review in order to compare the catalytic properties of Ru-based nanomaterials both for OER and HER.

3. Oxygen Evolution Reaction

RuO_2 NPs reported as catalysts for the OER have been prepared by diverse synthetic methodologies that exploit the rich redox chemistry of Ru. As main preparation methods one can cite (hydro)thermal,[29, 30, 31, 32, 33] and plasma-assisted[34, 35] methods starting both from $RuCl_3$, decomposition of molecular precursors under oxidative (usually electrocatalytic) conditions,[12] magnetron sputtering,[8] thermal[36,37,38,39,40]/ air[41]/ electrochemical[31] oxidation of pre-formed metallic Ru NPs, and chemical,[42] electrochemical[43] or photochemical[44] reduction of RuO_4^- species. Making use of the benchmarking parameters discussed in Section 2, the electrocatalytic performance of the most relevant Ru-containing nanoparticulated systems for the OER under acidic and basic conditions are summarized in Table 1 and Table 2, respectively. Graphical representations of η_{10}/b (where b is the slope of the Tafel plot, Figure 2) and TOF (Figure 3) for the same set of OER electrocatalysts are also provided and discussed along this section. As deduced from the black columns in Figure 2, most Tafel slopes are comprised between 50 and 60 mV·dec^{-1}, falling within the normal range observed for different metal oxides in the literature.[23]

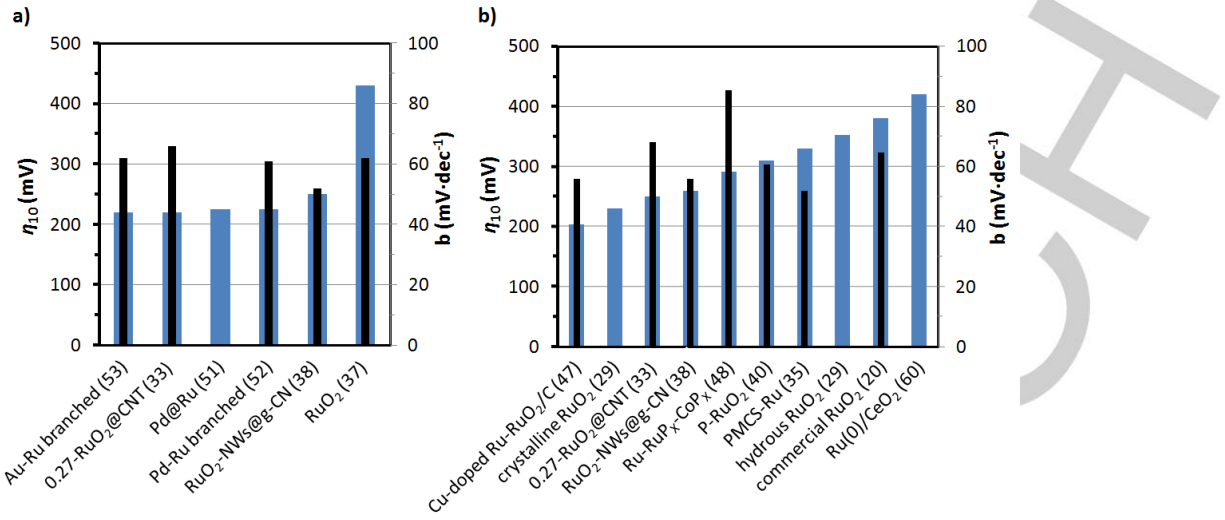

Figure 2. η10 (blue) and Tafel slope b (black) for the most relevant OER electrocatalysts in (a) acidic and (b) alkaline aqueous solution.

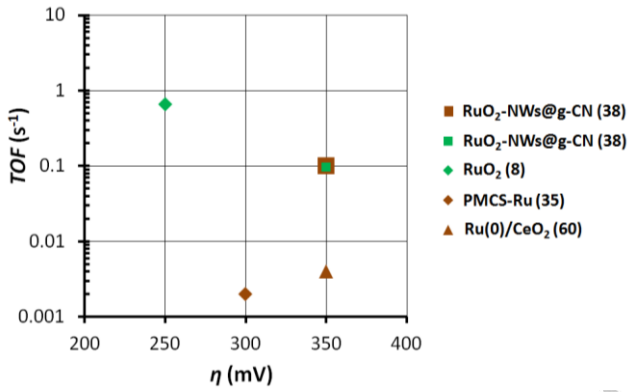

Figure 3. Graphical comparison of TOF vs. overpotential data for OER electrocatalysts in acidic (green) and alkaline (brown) aqueous solution.

3.1. Non-supported systems prepared *ex situ*.

A majority of the Ru-based nanocatalysts (either metallic Ru or RuO_2 NPs) assayed in the OER have been electrochemically triggered through deposition of the pre-catalytic entities onto RDE-GC. However, as noted above in Section 2, important difficulties arise when comparing the activity of the set of reported systems due to lack of homogeneity in electrode preparation methods, catalyst loadings and electrochemical test conditions. Thus, the following discussion will only focus on relevant contributions where benchmarked data are available, from which useful and accurate comparative information can be extracted.

A contribution from Stephens, Chorkendorff and co-workers[8] that constitutes one of the state-of-the art works and where the authors compare their results with other relevant data when appropriate is a good starting point to discuss about the factors ruling the activity and stability of Ru-based NPs in the OER. These authors carefully analyze the OER mass activity and stability (corrosion) in acidic media (0.05 M H_2SO_4) of both as-deposited and thermally oxidized (400 °C, 1 bar O_2, 1 min) Ru-based NPs prepared through magnetron sputtering. This preparation method allows a high control over the size (in the range 2-9 nm depending on the conditions applied) and mass of the particles together with very clean surfaces. Following the tendency observed for extended surfaces,[45] the activity of the as-deposited NPs (composed by a mixture of metallic Ru and RuO_2 as determined by XPS and XRD) is clearly higher than that of thermally oxidized NPs (identified as pure RuO_2). OER mass activity (0.6 A·mg^{-1}), specific activity (0.32 mA·cm^{-2}) and TOF (0.65 s^{-1} for η = 250 mV, Table 1, entry 1) data for the RuO_2 system were calculated from the known mass and surface area of spherical particles and compared with literature data. The different figures of merit listed above resulted one order of magnitude higher than those found for any other NP in acidic medium,[31,37,46] which is attributed by the authors to the clean surfaces provided by the preparation method. This is particularly clear when the performance of this system is compared with that of the chemically prepared 6 nm RuO_2 NPs reported by Shao-Horn and co-workers,[37] which have similar size and crystallinity but clearly lower specific activity (0.010 mA·cm^{-2}, Table 1, entry 2). Finally, the electroactivity of RuO_2 sites in the OER has been proven to be sensitive to the presence of heteroatoms (heteroatom inducement). A first example by Chen and co-workers reported very active Cu-doped Ru-RuO_2 NPs (Table 2, entry 5),[47] where, according to DFT calculations, the Cu doping allows tailoring the *d*-band centre of the RuO_2 active sites. A

second report on the same subject placed in good position a catalyst made of Ru/RuO_2 sites at the surface of Co_xP hollow polyhedra (Ru-RuP_x-Co_xP, Table 2, entry 6).[48] The high electrocatalytic OER performance observed is attributed to both the synergism of the two metals present and the high specific surface area of the hybrid nanomaterial.

Several authors have also studied the effect of the crystallinity degree of the employed Ru-based NPs on the OER.[29,36,43] Lim and co-workers[29] recently reported the inferior efficiency (η_0 123 mV higher) and stability of hydrous RuO_2 particles of low crystallinity with regards to those of its crystalline counterpart (prepared by annealing of the former at 300 °C) in 1 M KOH (Table 2, entries 2 and 3). In terms of overpotentials, this result differs from the results described for RuO_2 thin films.[49] The inverse trend is reported by Han and co-workers when analyzing metallic Ru NPs of different crystallinity.[36] The higher performance observed for amorphous Ru NPs has been attributed to the higher number of coordinatively unsaturated surface sites available in this type of material. Very recently, highly active partially hydrous 5 nm RuO_2 NPs embedded in a carbon matrix (x-RuO_2@C with x =hydration degree = 0.27) have been reported as OER electrocatalysts both at acidic and basic pH (Table 1, entry 7; Table 2, entry 8).[33] Their excellent OER activity has been related to the abundantly pre-existent hydroxyl species (-Ru-OH) in hydrous RuO_2, which possibly accelerate the deprotonation step to generate the oxyspecies (-Ru-O) necessary to form the Ru-OOH ones during the rds, together with the improved proton conduction throughout hydrous RuO_2. Thus, no clear trend can be extracted with the existent literature and more systematic research is desirable in this regard.

The stability of Ru-based NPs under OER conditions is another key issue to have at disposal durable electrodes for practical applications. When comparing the stability of their two systems, Stephens, Chorkendorff and co-workers[8] report important corrosion of the as-deposited Ru/RuO_2 NPs, observing dissolution from the electrode by electrochemical scanning tunneling microscopy (EC-STM), but relatively stable pure RuO_2 samples. This trend is in agreement with previous contributions that claim the higher stability of RuO_2 *vs.* Ru/RuO_2 NPs in the OER and the easy transformation of metallic Ru into RuO_4 under catalytic conditions (either acidic or basic) and consequently, its dissolution from the working electrodes.[7,31,37,50] Mechanistically, the work of Kötz *et al.*[50] describes the formation of a Ru^{VI} intermediate ($RuO_2(OH)_2$) from both Ru and RuO_2 at acidic pH prior to the formation of the RuO_4 species. Since the structure of the Ru^{VI} intermediate matches the crystal structure of RuO_2 and not that of Ru, the bonding with the former is stronger, thus decreasing its corrosion into RuO_4. Another particularly remarkable work is that of Strasser and co-workers,[31] where the electrocatalytic OER activity and stability of metallic Ru, Ir and Pt NPs is compared with that of their corresponding bulk counterparts. Even if Ru NPs show the best initial specific activity, important passivation and corrosion is observed from the first CV scan, forming water-soluble RuO_4 at potentials close to those needed for the OER. Remarkably, an alternative system for improving the stability of the Ru NPs while maintaining or even increasing their activity in the OER has been shown to be the combination of the Ru element with a more stable noble metal, less prone to undergo oxidation. Thus, Tilley and co-workers reported Pd@Ru core-shell NPs[51] or Pd-Ru[52] and Au-Ru[53] branched and faceted NPs, with η_{10} values of 220-230 mV and Tafel slopes of 61-62 mV·dec^{-1} in 0.1 M $HClO_4$ (Table 1, entries 4-6). The first work demonstrates that the Pd core stabilizes the Ru shell by up to ten times while maintaining the activity,[51] whereas the other two show that the presence of branches increases both the stability and activity of the NPs as compared to the respective bimetallic spherical systems.[52,53]

3.2. Systems arising from the decomposition of molecular complexes under OER conditions.

Contrasting with other transition metals (TMs), works describing Ru-based NPs for the OER generated under catalytic conditions from the oxidative decomposition of molecular complexes are scarce. This is in agreement with the intrinsic robustness of Ru molecular WOCs containing ligands that are not easily oxidized or, when properly designed, that are oxidized at a sufficiently slow rate so their degradation is negligible.[11] Among the most easily oxidizable organic substrates are those containing methylenic groups in benzyls, benzylalcohols and benzylpyridyls. Some complexes including these groups have been prepared, but a careful analysis of their behavior evidenced their degradation.[54,55,56] In fact, a detailed study by simultaneously measuring the amount of O_2 and CO_2 generated showed the formation of the latter from the very beginning. This implies that massive ligand degradation occurs together with the formation of O_2, and thus points to the formation of RuO_2 as the active species rather than the initial molecular complex. A relevant example of ligand degradation is the case of the complex [Ru(bda)(N-NH_2)$_2$] (bda^{2-} is [2,2'-bipyridine]-6,6'-dicarboxylate, N−NH_2 is 4-(pyridin-4-yl)aniline) anchored to a glassy carbon surface.[12] This is an extremely robust WOC in homogeneous phase that forms O-O bonds in a bimolecular manner *via* an intermolecular mechanism. Attached to the surface of a graphitic electrode, and therefore with restricted mobility, it cannot undergo dimerization. This involves accessing higher energy pathways to afford water oxidation, which in parallel facilitate ligand degradation. As a result, after a few catalytic cycles the only Ru species left at the electrode surface are RuO_2 NPs. With a TOF_i of 300 s^{-1} at Γ = 1.0 pmol·cm^{-2}, this system outperforms by several orders of magnitude the state-of-the-art systems prepared *ex situ* (see TOF data in Tables 1 and 2) and it has been incorporated in a photovoltaic-electrolyzer cell (PV-EC) together with an earth abundant cathode and a triple junction polymer cell, achieving solar to hydrogen conversion efficiencies of around 6%.[57] The reasons for the strikingly fast kinetics of this *in situ*-generated RuO_2 electrocatalyst still remain unraveled.

3.3. Supported systems.

As noted in Section 3.1, the deposition of NP-based systems onto electrode surfaces for the electrocatalytic assessment of their OER performance is a common practice. Therefore,

despite the use of electrodes is general, in most contributions they merely act as conducting supports for the colloidal catalysts. Hence, this section will only highlight contributions where the support is relevant for the catalytic performance of the catalyst and its role thoroughly discussed. Furthermore, in order to properly compare the reported results, it is useful here to group the systems on the basis of type of triggering energy used, which can be chemical, electrochemical or photochemical.

3.3.1. Chemical and electrochemical systems.

The preferably used chemical oxidant has clearly been Ce(IV), an outer-sphere one-electron oxidant with a high Ce(IV/III) redox potential, widely employed in the OER both for metal oxides and molecular catalysts. In this respect, Ren and co-workers reported the embedding of pre-formed 1.6 nm RuO_2 NPs into mesoporous silica (SBA-15, ≈ 6 nm pore size).[32] The so-obtained RuO_2@SBA-15 nanomaterial shows higher TOF than any reported system in SiO_2 (TOF_{max} = 0.27 s^{-1}) and a TON over 200 after recycling the catalyst more than 15 times. This high activity is attributed to a confinement effect of the RuO_2 NPs in the pores of the SBA-15 matrix, which prevents crystal growing during annealing and thus allows to get a metal oxide of small size and low crystallinity. Additionally, given the large pore size of the silica support, the catalyst presents a highly approachable surface area. This hypothesis is in agreement with the reduced activity reported for RuO_2 NPs of similar size when embedded in a mesoporous silica displaying pores as small as 2.7 nm (TOF_{max} of 0.038 s^{-1}),[58] probably because the smaller pores lead to a limitation of the active surface area exposure. Low TON and TOF values (10 and 0.006 s^{-1}, respectively) have been also recently obtained by Johnston and co-workers with sub-nanometric RuO_2 NPs embedded into a pyridine-functionalized siliceous mesocellular foam (MCF) arising from $RuCl_3$ impregnation onto the support, followed by reduction with $NaBH_4$ and air oxidation of the metallic Ru NPs formed.[41]

Martínez-Huerta and co-workers reported an electrochemically-triggered system prepared through the polyol method where the support/electrode has a key role for the described performance.[59] The system is bimetallic (Pt_3Ru) and supported onto titanium carbonitride (TiCN). The supported system, where a Ru/RuO_2 mixture catalyzes the OER, shows enhanced activity and stability when compared to unsupported RuO_2 NPs in acidic conditions. Both effects are attributed to the TiCN support that is able of delaying catalyst aggregation and dissolution thanks to the formation of a TiO_2 surface under turnover conditions. Also, Akbayrak, Önal and co-workers recently reported the facile preparation of a Ru(0)/CeO_2 system by chemically reducing CeO_2-impregnated Ru^{3+} ions with $NaBH_4$.[60] The hybrid system electrochemically catalyzes the OER at modest overpotentials (η_{10} = 420 mV) and TOF values (0.004 s^{-1}) but is nearly stable for 1000 CV cycles in 0.5 M KOH (Table 2, entry 10). No analysis of the surface oxidation state evolution under OER conditions is provided. Finally, Zou and co-workers have recently reported a relevant OER electrocatalyst arising from the pyrolysis of a bimetallic CuRu-MOF, forming Cu/Ru NPs onto a hierarchically porous carbon (HPC) matrix, followed by Cu NPs etching and thermal oxidation of the metallic Ru NPs (Ru-HPC) into RuO_2 NPs (P-RuO_2).[40] The 5.64 nm average size P-RuO_2 system shows improved OER performance in 1.0 M KOH (η_{10} = 310 mV, b = 60.7 mV·dec^{-1}, Table 2, entry 11) when compared to commercial RuO_2 (Table 2, entry 7) and is particularly interesting due to its stability (no sign of deactivation after 2000 CV cycles). The hierarchically porous structure of the hybrid material, which leads to a high exposure of the surface RuO_2 active sites as demonstrated through BET and ECSA analysis, is proposed as the origin of its superior activity.

3.3.2. Photochemical systems.

In order to photo-catalytically test Ru-containing NPs in the OER, systems based on $[Ru(bpy)_3]^{2+}$ as photosensitizer (PS) and $S_2O_8^{2-}$ as sacrificial electron-acceptor (SEA) have been most commonly employed.[41,42, 61] However, the use of semiconducting materials as light-harvesters has also been reported.[30] Ren and co-workers provide a noteworthy example when photo-catalytically evaluating a 2nd generation (with a better dispersed Ru phase) of their RuO_2@SBA-15 system (see Section 3.3.1. above). They reported O_2 yields over 90%, quantum efficiencies of *ca.* 10% and a TOF value of $2.7 \cdot 10^{-2}$ s^{-1} when combining their nanomaterial with $[Ru(bpy)_3]^{2+}$ as PS and persulfate as SEA (Figure 4).[61] This system outperforms many other metal oxides based on different TMs and the rest of light-driven RuO_2 systems reported to date, being recycled up to 5 times with minimal loss of activity. The authors attribute again the high activity observed to the large pores of the SBA-15 support, which allows an efficient interaction between the catalyst and the PS. Also, Johnston and co-workers[41] reported the photocatalytic evaluation of their MCF-based system (*vide supra*). With a similar OER configuration, they attained a TON of 4 (moles of produced O_2 per mole of Ru) and one order of magnitude lower TOF of $2.2 \cdot 10^{-3}$ s^{-1}. A different approach that aimed at facilitating electron transfer between the RuO_2 catalyst and the PS was reported by Yoshida and co-workers.[42] The described hydrogel system closely arranges pre-formed RuO_2 NPs and a $[Ru(bpy)_3]^{2+}$-derivative by means of both electrostatic interactions between polar groups and steric confinement within a poly(N-isopropyl)acrylamide polymeric matrix. A sustained production of oxygen was observed when the system was combined with $[Co(NH_3)_5Cl]^{2+}$ as SEA and irradiated with visible light. Finally, Domen and co-workers have used an n-semiconductor TaON material doped with RuO_2 NPs of different sizes arising from the calcination of $[(NH_4)_2RuCl_6]$ at different temperatures.[30] This RuNP-doped TaON system was compared with bare TaON under visible light irradiation and the presence of $S_2O_8^{2-}$. The obtained results highlight the higher efficiency of the RuO_2-based nanomaterial as OER photocatalyst and the critical role that the good dispersion of the metal oxide has on the catalytic performance.

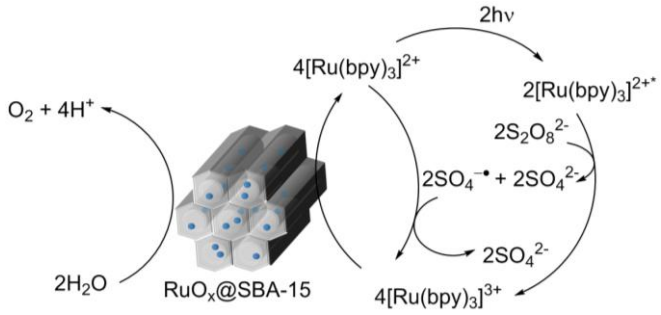

Figure 4. RuO_2@SBA-15 system designed for OER photocatalysis in the presence of $[Ru(bpy)_3]^{2+}$ as PS and persulfate as SEA reported by Ren and co-workers. Adapted from ref. [61].

Table 1. Comparison of the most relevant Ru-based OER nanoelectrocatalysts under acidic conditions. Parameters: mean diameter (Ø), onset overpotential (η_0, mV), overpotential at $|j|$ =10 mA·cm^{-2} (η_{10}, mV), Tafel slope (b, mV·dec^{-1}), specific current density ($|j_S|$, mA·cm^{-2}) and turnover frequency (TOF, s^{-1}). Unless otherwise stated, electrolyte is 0.5 M H_2SO_4.

Entry	Catalyst	Ø (nm)	η_0 (mV)	η_{10} (mV)	b (mV·dec^{-1})	$\|j_S\|$(mA·cm^{-2})	TOF (s^{-1})	Ref.
1	RuO_2 [a]	3-5	≈ 185	-	-	0.32 (250 mV)	0.65 (250 mV)	8
2	RuO_2 [b]	≈ 6	≈ 220	430	62	0.010 (250 mV)	-	37
3	RuO_2-NWs@g-CN	10-40	200	250	52	-	0.0961 (350 mV)	38
4	Pd@Ru [b]	≈ 6 @ 0.5	≈ 120	220-230	-	0.02 (≈250 mV)	-	51
5	Pd-Ru branched [b]	6.1 x 9.1	≈ 170	225	61	-	-	52
6	Au-Ru branched [b]	≈ 9.0 x 8.5	≈ 160	220	62	0.3 (230 mV)	-	53
7	0.27-RuO_2@C	5	≈ 170	220	66	-	-	33

Electrolyte: [a] 0.05 M H_2SO_4 and [b] 0.1 M $HClO_4$.

Table 2. Comparison of the most relevant Ru-based OER nanoelectrocatalysts under basic conditions. Parameters: mean diameter (Ø), onset overpotential (η_0, mV), overpotential at $|j|$ =10 mA·cm^{-2} (η_{10}, mV), Tafel slope (b, mV·dec^{-1}), specific current density ($|j_S|$, mA·cm^{-2}) and turnover frequency (TOF, s^{-1}). Unless otherwise stated, electrolyte is 1.0 M KOH/NaOH.

Entry	Catalyst	Ø (nm)	η_0 (mV)	η_{10} (mV)	b (mV·dec^{-1})	$\|j_S\|$(mA·cm^{-2})	TOF (s^{-1})	Ref.
1	RuO_2 [a]	≈ 6	≈ 220	-	84	0.003 (250 mV)	-	37
2	hydrous-RuO_2	< 5	≈ 290	353	-	-	-	29
3	crystalline-RuO_2	-	≈ 170	230	-	-	-	29
4	RuO_2-NWs@g-CN [b]	10-40	190	260	56	-	0.0995 (350 mV)	38
5	Cu-doped Ru-RuO_2/C	2.5-4.5	≈ 155	204	56	-	-	47
6	Ru-RuP_x-Co_xP [a]	2.4	≈ 240	291	85.4	-	-	48
7	commercial RuO_2	50-100	-	380 ± 20	64.6	0.078 (350 mV)	-	20

8	0.27-RuO_2@C	5	≈ 200	250	68	-	-	33
9	PMCS-Ru[c]	2.6	≈ 260	330	52	-	0.002 (300 mV)	35
10	Ru(0)/CeO_2[b]	-	340	420	122	-	0.004 (350 mV)	60
11	P-RuO_2	5.64	≈ 260	310	60.7	-	-	40

Electrolyte: [a] 0.1 M KOH and [b] 0.5 M KOH. [c] PMCS stands for pulsed microplasma cluster source.

4. Hydrogen Evolution Reaction

The application of Ru-based nanocatalysts for the HER is a recent but fast-evolving field, with most of the relevant literature published in the 2016-19 period. Even if some photocatalytic examples exist (see Section 4.4 below), most of the reported systems are mainly constituted of Ru NPs deposited or supported/embedded onto conductive C-based (or even metallic) materials that are electrochemically triggered. The following sub-sections will thus emphasize the most outstanding nanomaterials reported and, particularly, the reasons that make them excel. A comparison of the most relevant HER electrocatalytic data of Ru-based nanoparticulated systems under acidic and basic conditions is given in Table 3 and Table 4, respectively. Additionally, graphical representations of η_{10}/b (where b is the slope of the Tafel plot, Figure 5) and TOF (Figure 6) for the same set of HER electrocatalysts are also provided and discussed along this section. As can be seen from the black columns in Figure 5, most Tafel slopes are comprised within a 30-40 mV·dec^{-1} range, thus indicating either Heyrovsky or Tafel step as the rds. However, some values stand above 40 mV·dec^{-1} (up to 70 mV·dec^{-1}), either due to experimental inaccuracy and/or to the reported dependence of b with applied potential.[25]

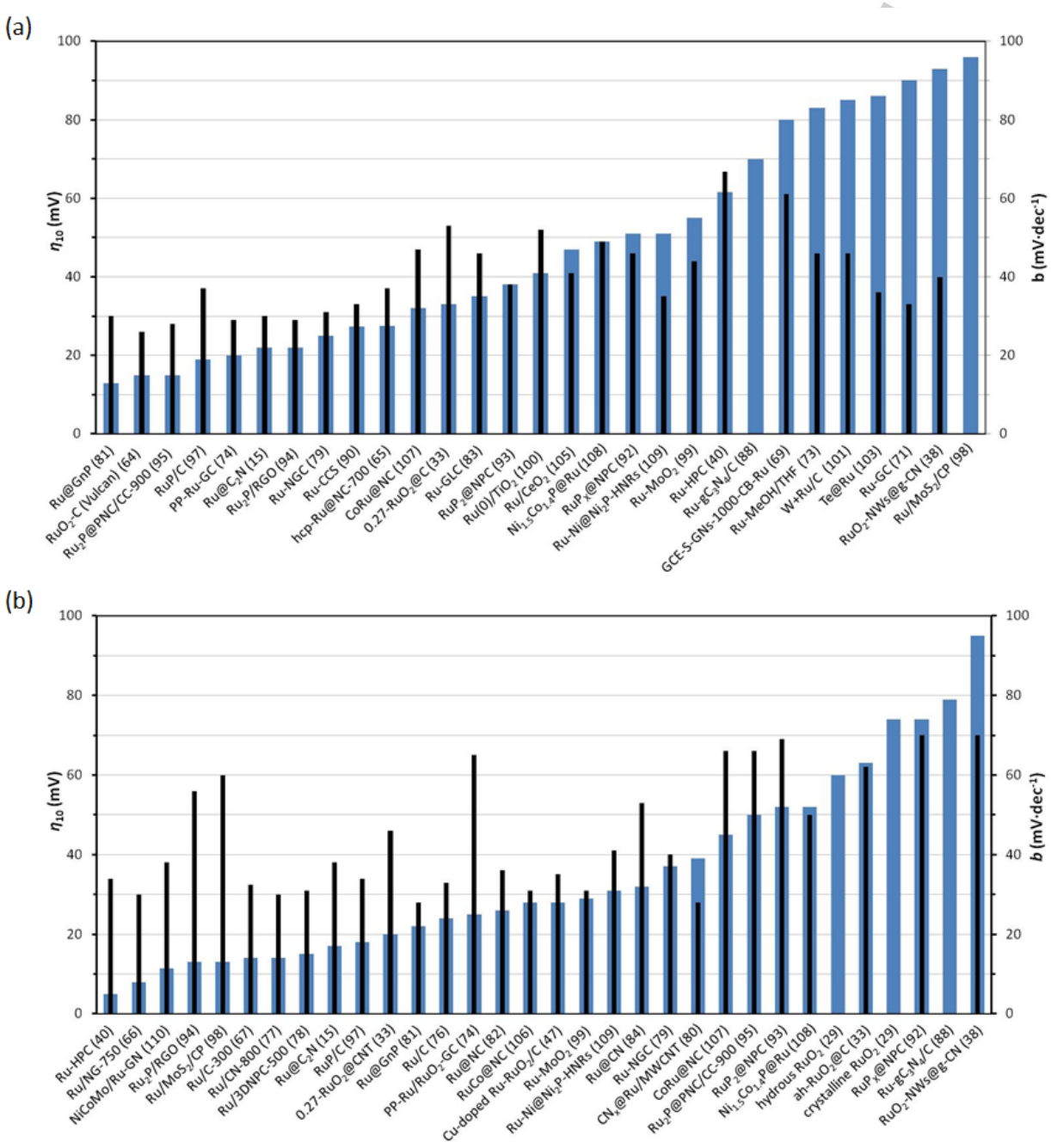

Figure 5. η_{10} (blue) and Tafel slope b (black) for the most relevant HER electrocatalysts in (a) acidic and (b) alkaline aqueous solution.

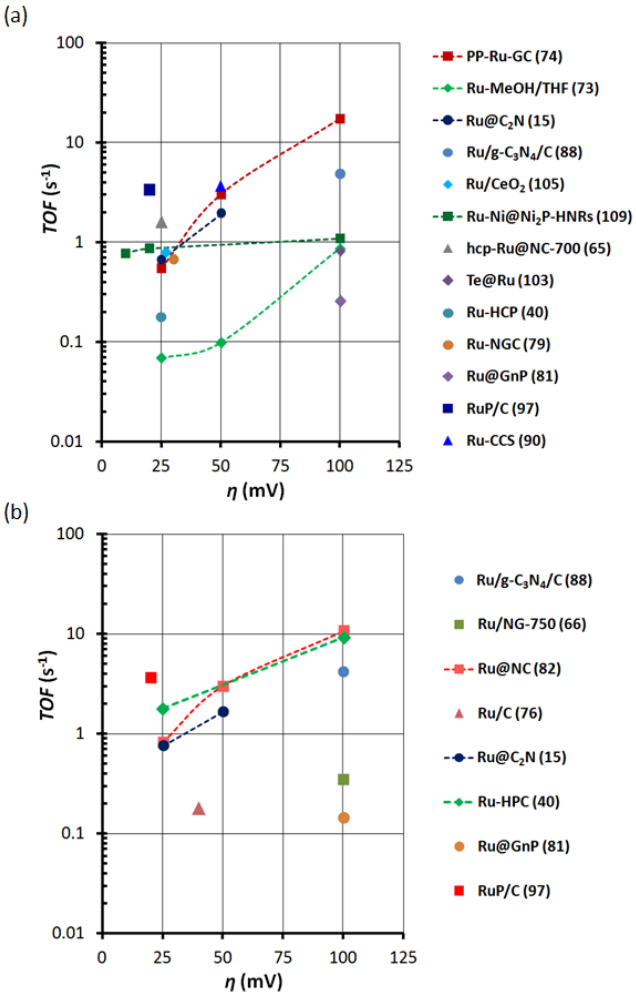

Figure 6. Graphical comparison of TOF vs. overpotential data for HER electrocatalysts in (a) acidic and (b) alkaline aqueous solution.

4.1. Non-supported electrochemical systems prepared *ex situ.*

Analogously to OER electrocatalysts, Ru-based nanoparticulated HER electrocatalysts have been prepared *ex situ* and then deposited onto the surface of C-based materials (but also Ni foam or even silver epoxy), in order to facilitate electronic transfer under catalytic turnover and easily assess their electrocatalytic performance. In the majority of the cases the supporting electrode does not modify the intrinsic catalytic properties of the Ru-based NPs and it is in this sense that these systems have been considered as 'non-supported' in this section. Contrasting with the `supported' systems that will be described in Section 4.2, where the supports used frequently dictate the catalytic performance and where the compositional complexity leaves hardly any space for the fine-tuning of the active sites, the non-supported systems such as those presented in this section are potentially better positioned in this regard.

Non-supported Ru-based NPs have been prepared through a myriad of methods such as the thermal decomposition/calcination of anhydrous RuO_2,[62] a Ru salt[29, 63, 64, 65] or a Ru complex,[39,66,67] or through the electro-reduction of a Ru salt,[68, 69] Ru perovskite-type precursor[70] or Ru complex.[71] However, the tailored synthesis and rational catalytic fine-tuning of non-supported Ru-based NPs is not a simple matter. First, the use of a stabilizer (typically a coordinating solvent, a ligand or the surface of a material) is mandatory in order to hold the systems at the nanoscale, preventing the formation of thermodynamically favored bulk species. Second, the metal oxidation state at the NP surface may evolve and even reversibly switch (typically between metallic Ru and Ru(IV) in RuO_2) when in contact with air and/or under (electro)catalytic turnover conditions (see below). Thus, having at disposal an effective way to synthesize Ru-based NPs with controlled size, shape, oxidation state and surface composition is of utmost interest. In this regard, the so-called organometallic method, based on a controlled decomposition under mild conditions (e.g. 3 bar of H_2, r.t.) of an organometallic olefinic Ru precursor in the presence of a stabilizing agent (often a ligand) is particularly well-suited, yielding clean surfaces and a set of surface hydrides that can be easily titrated.[72] In addition, the ligand added for the synthesis and present on the surface of the NPs may play a key role on the overall HER activity of the nanocatalysts, potentially influencing the electronic properties of the NP surface, the number and disposition of the active (hydridic) sites available and even the mechanistic pathways through which H_2 is formed. This resembles the characteristics of molecular metal-organic compounds in catalysis and makes such Ru NPs highly interesting systems for finely studying their catalytic properties in HER. As a first result, we have recently published significantly active Ru NPs stabilized in MeOH/THF and deposited onto GC electrodes.[73] This catalytic system demonstrated the advantages of using the organometallic approach to obtain highly homogeneous NPs with very high active surface areas free of strongly coordinated stabilizers. Thus, the 21.4 nm porous Ru NPs show in 0.5 M H_2SO_4 $\eta_0 \approx 0$ mV, $\eta_{10} = 83$ mV, a Tafel slope of 46 mV·dec^{-1}, a $TOF_{100\ mV}$ of 0.87 s^{-1}, a Faradaic efficiency of 97% and excellent durability up to 12 h (Table 3, entry 19). Also, more recently, we have synthesized very small 4-phenylpyridine(PP)-capped Ru NPs (mean size 1.5 nm),[74,75] which have been afterwards drop-casted onto a GC electrode for electrochemical analysis (PP-Ru-GC) and thoroughly characterized under air and HER turnover conditions in both acidic and basic conditions. The surface of these Ru NPs spontaneously oxidizes to RuO_2 upon air exposure, yielding a mixed Ru/RuO_2 system where the PP ligand is still present. Although this mixed Ru/RuO_2 system is less active towards HER compared to pure Ru NPs, it can be converted into the metallic Ru form under reductive conditions (20 min-bulk electrolysis at -10 mA·cm^{-2}) at acidic pH (Figure 7).[74] Thus, the recovered PP-Ru-GC system exhibits $\eta_0 \approx 0$ mV, $\eta_{10} = 20$ mV, a Tafel slope of 29 mV·dec^{-1} and a TOF as high as 17.4 s^{-1} at $\eta = 100$ mV in 1 M H_2SO_4, showing complete stability after 12 h of continuous operation (Table 3, entry 25). A similar activation process under reductive potentials (but tentatively attributed to RuO_2 structure

deformation) had been previously reported by Zhang et al. for C-supported 5-8 nm RuO_2 NPs,[64] which formed a very active HER electrocatalyst at acidic pH ($\eta_0 \approx 0$ mV, $\eta_{10} \approx 15$ mV and Tafel slope of 26 mV·dec^{-1}; Table 3, entry 1). Despite being out of the nanoscale domain, the phase transformation of the RuO_2 coating (0.4-1.4 μm) of RuO_2/Ni electrodes, first into $RuO(OH)_2$ and then into metallic Ru under hydrogen evolution conditions, has also been reported by Näslund and co-workers through a careful analysis combining XRD and XPS.[63] In contrast, in 1 M NaOH the only stable form of our PP-Ru-GC system is the mixed Ru/RuO_2 form, yielding a slightly less active and stable system, although still outperforming the performance and stability of commercial Pt/C (Table 4, entry 26). We proposed that the presence of the PP capping agent induces good mechanical stability, thus allowing the maintenance of the nanostructured character of the material even after a long run. This hypothesis is supported by DFT calculations, which show the coordination of eleven PP molecules onto the surface of a $Ru_{55}H_{53}$ NP both through N-σ and π-coordination modes, the latter being more stable and preferentially taking place on the edges of the NP. Furthermore, the d-band energy levels of the surface Ru atoms are significantly modified by the presence of hydride ligands, which have a stabilizing effect, whereas these energy levels are not significantly altered by the PP capping ligands, thus indicating a moderate adsorption strength of the latter onto the NP surface. In consequence, a larger number of hydride ligands are present on the NP surface compared to PP (53 vs. 11), thus accounting for its enhanced H_2 evolution behavior.

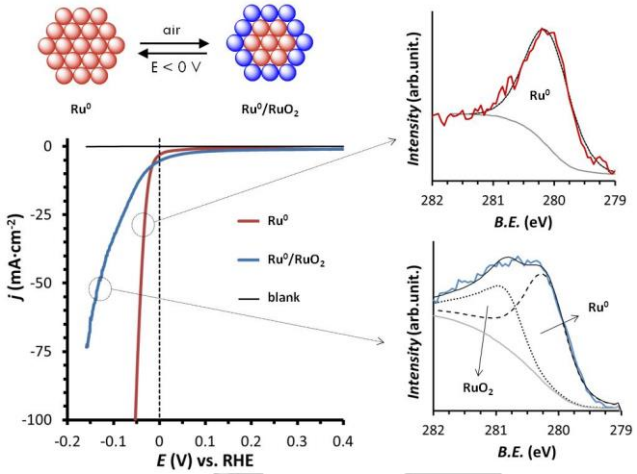

Figure 7. Polarization curves in a 1 M H_2SO_4 solution at 10 mV·s^{-1} and XPS data of metallic PP-Ru NPs and their Ru(0)/RuO_2 surface-passivated counterpart formed upon air exposure. Adapted from ref. [74].

In terms of scalable and cost-effective methods for the production of active Ru-based nanoparticulated systems for the HER, Fan, Hu and co-workers have recently reported the solid-state synthesis of Ru NPs. These NPs were simply prepared by mixing at room temperature $RuCl_3$, NaOH, $NaBH_4$ and a C source in an agate mortar.[76] This led to very active, stable and homogeneous in size (1.7 nm) Ru NPs deposited onto C (Ru/C) that show η_{10} = 24 mV and a Tafel slope of 33 mV·dec^{-1} at pH 14 (Table 4, entry 27), thus improving again the performance of commercial Pt/C in alkaline solution.

The degree of crystallinity is another critical issue ruling the activity and stability of nanoparticulated non-supported Ru-based HER electrocatalysts that, as stated above for the OER, has not been thoroughly studied. Concerning RuO_2 NPs, the works of Lim et al.[29] and Song et al.[33] show both a clear decrease of the HER activity after increasing the crystallinity of their initially hydrous RuO_2 NPs through annealing processes (see Table 4, comparison between entries 3 and 4 and entries 31 and 32, respectively). A word of caution: the surface oxidation state of the nanomaterial (initially Ru(IV) in RuO_2) has not been analyzed after catalytic turnover under reductive conditions and thus the reduction to metallic Ru (as demonstrated in refs. 63 and 74 and discussed above) acting as the true active species cannot be discarded. A single very recent report by Qin, Bu, Liu and co-workers deals with the issue of crystallinity of metallic Ru NPs.[65] The authors highlight the gradual increase in the HER activity of their Ru@NC system (NC = N-doped C) as the annealing temperature is increased up to 700 °C. The 700°C-annealed catalytic system displays high activity (η_{10} = 27.5 mV, a Tafel slope of 37 mV·dec^{-1} and a TOF of 1.6 s^{-1} at η = 25 mV calculated through ECSA values, Table 3, entry 30) and durability (up to 6 h and 20000 CV cycles) in acidic conditions. DFT calculations show a gradual increased exposure of the more efficient (100) and (002) surfaces during the temperature-induced crystallization process as the reason for the increased activity of the highly crystalline hcp Ru NPs. Thus, the available data on non-supported systems point to amorphous RuO_2-based NPs and highly crystalline Ru NPs as the species of choice for attaining high performance HER nanoparticulated electrocatalysts.

4.2. Supported electrochemical systems on C-based/composite C-based materials.

In agreement with the definition of "non-supported" systems given in Section 4.1, the term "supported" here concerns Ru-based nanoparticulated HER electrocatalysts where the support employed dictates (or markedly influences) the catalytic performance. As the section title suggests, the systems presented are based on either simple carbon supports (e.g. graphene) or more complex C-based multi-element composite materials (see below), where the Ru NPs are typically integrated by annealing a Ru precursor (usually a Ru salt or complex).

A first set of catalytic systems deals with the deposition of Ru NPs onto a conductive carbon-based matrix (e.g. carbon nitride, graphene or N-doped graphene, hollow carbon spheres, etc.) through annealing of a Ru precursor. A relevant example by Tour and co-workers deals with Ru-nanoclusters deposited onto N-doped graphene.[66] Their catalytic systems, prepared by nucleation of $[Ru(NH_3)_6]^{3+}$ as Ru precursor on graphene oxide (GO) at 160 °C followed by reduction under NH_3/Ar at different temperatures (350-850 °C), contain Ru nanoclusters of different

average sizes, Ru average oxidation states, N contents, BET surface areas, pore size distributions and HER activities depending on the reducing temperature. Although slightly unstable under acidic HER conditions (probably due to dissolution), under alkaline conditions (pH 14) the 5.8 nm nanoclusters formed at 750 °C showed impressive activity and stability (for 4000 LSV cycles), with η_0 = 0 mV, η_{10} = 8 mV and a Tafel slope of 30 mV·dec^{-1} (Table 4, entry 6). DFT calculations support the better performance of the system in alkaline HER conditions, which is attributed to the high Ru-H_2O binding energy at this pH and the corresponding increase of the H_2O capture rate at the metal surface. The key role of N-doping in C-supported Ru nanoparticulate HER electrocatalysts in alkaline conditions is also supported by two recent contributions by Zhang, Fan and co-workers.[77,78] These reports introduce N-doping to C-black and 3D carbon supports through the pyrolysis of a $[Ru(bpy)_3]^{2+}$ complex[77] or $RuCl_3$/urea,[78] respectively, yielding *ca.* 1.3 nm supported Ru NPs in both cases as best performing systems. Both electrocatalysts show low HER overpotentials (η_{10} =14-15 mV) and relatively high stabilities in 1.0 M KOH (1000 CV cycles) that outperform those of Pt/C (Table 4, entries 14 and 15). A thorough comparison with the corresponding undoped systems highlights the importance of N to avoid aggregation and boost the electrocatalytic activity. Analogously, N-doping of graphite C (NGC) has been an excellent strategy to boost the HER activity of Ru NPs both at acidic and basic pH (Table 3, entry 15; Table 4, entry 16),[79] and the beneficial effect of a C nitride coating onto Ru NPs deposited on MWCNTs has been recently reported at pH 14 (Table 4, entry 17).[80] However, in a recent paper the HER activity of Ru NPs deposited onto graphene nanoplatelets (Ru@GnP; Table 3, entry 16; Table 4, entry 18)[81] has been shown to decrease after N-doping due to the blocking of Ru active sites by N atoms. Excellent HER performance in alkaline conditions has also been recently reported by Yamauchi and co-workers by means of a hierarchically ordered system.[82] As shown in Figure 8, the catalyst is prepared by a potential-controlled (-0.2 V vs. SCE) assembly of $[Ru(CN)_6]^{4-}$ units into the *diluted* oxidized units of a polyaniline fiber foam deposited onto carbon paper followed by a carbonization process at 900 °C. Monodisperse 1.6 nm Ru nanoclusters are thus deposited onto the surface of the N-doped C support (Ru@NC). Very good HER activity and stability in alkaline solution (pH 14) were obtained with this nanomaterial at particularly low Ru loading (2% wt), showing a η_{10} of only 26 mV, a Tafel slope of 36 mV·dec^{-1} and an impressive TOF_{100mV} of 10.8 s^{-1}, as well as an excellent stability after 12 h or 10000 cycles (Table 4, entry 13). Interestingly, its mass activity at η = 100 mV (17 A·mg^{-1} Ru) is 6.8 times that of a commercial Pt/C catalyst displaying a Pt loading of 20%. These comparative results evidence the importance of the location of the metallic NPs on the support: deposition onto the surface of the conductive C support and not inside the C matrix where the reaction may be hampered leads to better activity. A second prominent hierarchical composite HER electrocatalyst is Ru-HPC[40] arising from the pyrolytic decomposition of a CuRu-MOF, the oxidized version of this system (P-RuO_2) has already been discussed as an OER electrocatalyst in Section 3.1.1 (see above). In 1.0 M KOH, the Ru-HPC composite clearly outperforms commercial 20% Pt/C, achieving η_{25} = 22.7 mV, η_{50} = 44.6 mV, a Tafel slope of 33.9 mV·dec^{-1} and a TOF_{25mV} of 1.79 s^{-1} (Table 4, entry 19), showing total stability after 10 h of continuous operation. The bimetallic MOF-templated synthetic strategy adopted by the authors is at the core of the outstanding results obtained and it relays on (a) the uniform distribution and adjustable concentration of Ru sites in the CuRu-MOF precursor employed, (b) the Cu etching strategy applied resulting in an increased exposition of Ru active sites and (c) the high surface area and highly porous nature of the hierarchical C-based structure formed. Ru-HPC has also been tested in acidic media (0.5 M H_2SO_4) but the obtained results are average among Ru-based nanomaterial electrocatalysts (Table 3, entry 17). Comparable catalytic results that outperform the HER activity of commercial Pt/C in alkaline solution have been obtained by Zhang and co-workers by using a catalyst made of 1.5 nm Ru NPs onto C prepared upon adsorption of $[Ru_3(CO)_{12}]$ on the C-matrix followed by pyrolysis at 300 °C (Ru/C-300).[67] In 1.0 M KOH, the Ru/C-300 nanomaterial achieves $\eta_0 \approx 0$ mV, η_{10} = 14 mV and Tafel slope of 32.5 mV·dec^{-1} (Table 4, entry 25), showing almost total stability after 1000 cycles as the result of the deposition of the Ru NPs onto the C matrix. Furthermore, this work demonstrated that the pyrolysis temperature affects the size and dispersion of the NPs formed, which in turn modifies their HER catalytic activity. As a conclusion, the favorable H_2O binding/dissociation energies make Ru outperform Pt under alkaline conditions. Conversely, Adschiri *et al.* showed the relatively similar behavior of the two metals in acidic conditions when analyzing the HER activity of 2-5 nm Ru NPs onto graphene-layered carbon (GLC) (Table 3, entry 4) through both experimental and computational data.[83]

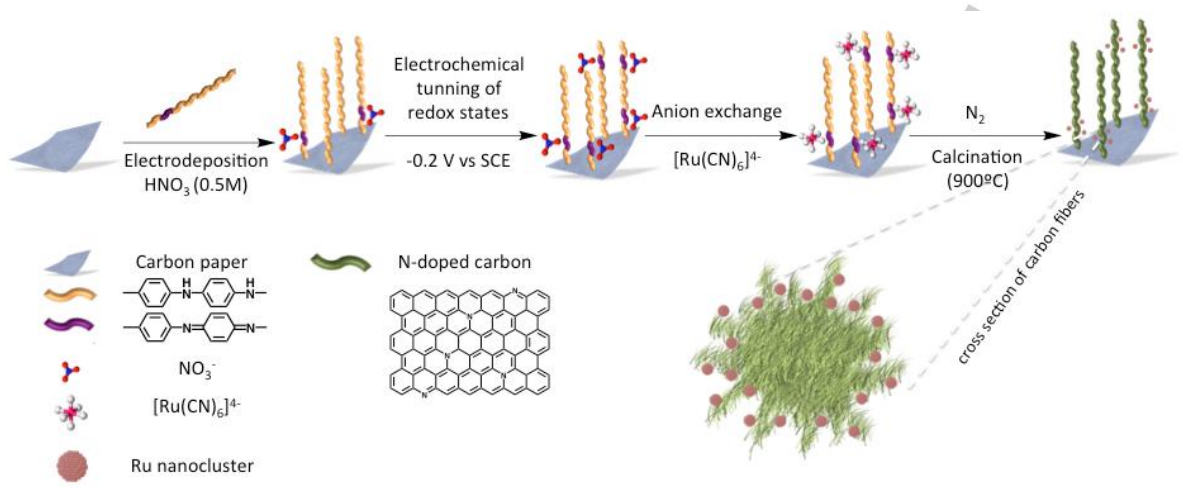

Figure 8. Schematic representation of the synthesis of the hierarchically-ordered N-doped carbon electrode containing 1.6 nm hcp-Ru nanoclusters (Ru@NC) reported by Yamauchi *et al*.[82] Color code: reduced polyaniline fibers, yellow; oxidised polyaniline fibers, violet.

A second relatively wide set of supported systems are those prepared by co-pyrolysis of C, N and Ru sources. Thus, Wang and co-workers obtained 2.4 nm Ru NPs onto N-doped graphene-like nanosheets (Ru@CN) by co-pyrolysis of glucosamine, melamine and $RuCl_3$.[84] Their Ru@CN system shows $\eta_0 \approx 0$ mV and $\eta_{10} = 32$ mV at pH 14 and also excellent stability after 2000 CVs (Table 4, entry 12). This catalyst displays a 9 times higher mass activity than that of commercial Pt/C while keeping 90% of the initial activity after 10 h of continuous operation at 60 °C. The authors attribute this behavior to the strong interaction between Ru and N sites on the support, which avoids agglomeration and leaching of the Ru NPs. However, this system shows moderate activity at acidic (Table 3, entry 14) and neutral pH. Additionally, the strong effect of a composite carbon matrix prepared by a co-pyrolysis method in the Ru-H/OH/H_2O binding energies and H_2O dissociation rates and, thus, in the HER electroactivity of the corresponding Ru NPs through the entire pH range has been emphasized by a prominent work of Baek and co-workers.[15] They prepared a material made of 1.6 nm hcp-Ru NPs embedded into a nitrogenated holey two-dimensional carbon structure (Ru@C_2N) by polycondensation of hexaketocyclohexane and hexaaminobenzene in the presence of $RuCl_3$, followed by a subsequent reduction with $NaBH_4$ at 175 °C. The so-obtained Ru@C_2N catalyst showed excellent HER performance both at acidic pH (with $\eta_{10} = 22$ mV and a Tafel slope of 30 mV·dec^{-1}; Table 3, entry 7) and at basic pH (with $\eta_{10} = 17$ mV and a Tafel slope of 38 mV·dec^{-1}; Table 4, entry 2), improving the values for Pt/C at pH 14. Furthermore, the HER catalytic activity at acidic pH rises after 1000 cycles, reaching a η_{10} of only 13.5 mV. DFT calculations on Ru_{55} models revealed the key role of the C_2N framework for the high electrocatalytic activity of the nanomaterial. In alkaline conditions, a significant increase of both the Ru-OH_2 binding energy (leading to faster water adsorption) and the rate of water dissociation (yielding faster proton supply) is observed. These effects, triggered by the C_2N matrix, compensate the unfavorably high OH binding energy on Ru (compared to Pt) and increase its efficiency in the Volmer reaction and thus its whole HER efficiency. The beneficial effects of C_2N-type of substrates in water splitting electrocatalysis, including stability against aggregation and high electroactivity, have also been raised by Zhou and co-workers by means of first-principles computations of a series of transition metal atom anchored C_2N monolayers, including Ru_x@C_2N species.[85] A word of caution: individual ruthenium atoms embedded into C_xN_y matrices have been recently identified as the true catalytic sites for HER in alkaline media, even if formed together with Ru NPs through co-pyrolysis synthetic methods.[86, 87] These works emphasize the importance of structurally characterizing new electrode materials at atomic scale in order to unravel the nature of the real catalytic active species present.

It is noteworthy that despite metallic Ru usually adopts a hcp structure, different groups observed that the co-pyrolysis synthetic method led to either hcp, fcc or mixed hcp/fcc Ru phases in the final NPs.[47, 88, 89] Assessment of the HER electroactivity of these systems evidences the positive influence of the fcc-Ru phase onto the final catalytic behavior in alkaline conditions (Table 4, entries 5 and 28). For example, Qiao and co-workers prepared fcc-structured 2 nm Ru NPs on graphitic carbon nitride (g-C_3N_4/C) starting from dicyandiamide and $RuCl_3$.[88] When drop-casted onto RDE-GC, the so-obtained Ru/g-C_3N_4/C nanomaterial showed significant activity (η_0 = 15-20 mV) and stability for 50 h (Table 4, entry 5), outperforming commercial Ru/C and Pt/C under identical conditions. The authors attributed these results to the atypical Ru structure that might be induced by the *g*-C_3N_4 support. As shown in Figure 9, this hypothesis is supported by theoretical data only when both thermodynamics (adsorption energies) and kinetics (water dissociation rates) are considered as activity descriptors.

Thermodynamically, DFT calculations on selected metal surfaces showed H adsorption energies (ΔG_{H^*} in Figure 9) following the Pt < Ru_{fcc} < Ru_{hcp} trend. Thus, with the lowest Ru-H strength, from the thermodynamic point of view Pt should show the highest HER activity. However, fcc-Ru shows the lowest water dissociation barrier (ΔG_B in Figure 9) among the three studied systems, while Pt shows the highest. Thus, the kinetics of water dissociation are favored for fcc-Ru at basic pH, which results key for the observed HER performance. This work evidences the relevance of considering the kinetics of water dissociation when modeling the HER performance of Ru-based nanocatalysts in alkaline media.[88]

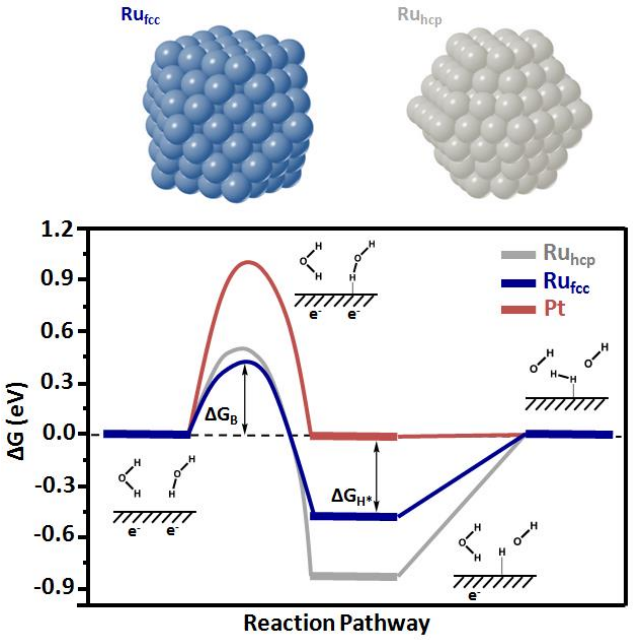

Figure 9. Top: Representation of the anomalous fcc-Ru phase (left) and the habitual hcp-Ru phase (right). Bottom: Gibbs free energy diagram of HER on Ru_{fcc} (blue), Ru_{hcp} (grey) and Pt (red) surfaces as reported by Qiao *et al*. [88]. ΔG_{H^*} corresponds to H adsorption free energy and ΔG_B corresponds to water dissociation free energy barrier. Adapted from ref. [88].

The beneficial effect of introducing heteroatoms onto the coordination sphere of Ru has also been demonstrated. For example, hcp-Ru NPs onto a carbonized collagen scaffold (Ru-CCS; Table 3, entry 8) by co-assembly of collagen and $RuCl_3$ and subsequent pyrolysis at 800 °C under Ar[90] show coordination to P and S atoms, which according to DFT calculations promote separation of electrons and holes and increase the amount of localized electrons on Ru, therefore facilitating proton adsorption by lowering ΔG_H^* close to zero. In this sense, the introduction of phosphorous into HER nanoparticulated electrocatalysts using phosphide containing transition metal NPs has been another common strategy. It is a way to take advantage of both the moderate H binding energy of P and the increase in corrosion resistance of the nanomaterials at acidic pH induced by the P presence, the latter improving their stability.[91] Thus, for Ru NPs, the introduction of P has been shown as extremely productive in HER catalysis in acidic conditions, but also at neutral and basic pH, normally generating composite systems in which the effect of the C-based material has also been proven essential for preventing the aggregation and tuning the electronic properties of the NPs.[92,93,94,95] For example, very stable HER catalytic systems at all pHs have been obtained by encapsulating RuP_x NPs inside N,P-doped C shells[93] (RuP_2@NPC; Table 3, entry 13; Table 4, entry 11) and nanospheres[92] (RuP_x@NPC; Table 3, entry 9; Table 4, entry 7). Two highly active system concerning the use of these pH-versatile RuP_x NPs in C-based supports have been recently reported by Chen, Hu *et al.*[94] and Li, Hu *et al.*,[95] in which the synergistic interaction between the NPs and the C-based support provokes an increase in electron mobility and a charge density redistribution between them, the latter inducing an optimal H adsorption energy close to 0 and thus highly active HER electrocatalysts. In the first work, < 7 nm Ru_2P NPs were deposited onto reduced graphene oxide (Ru_2P/RGO) after a thermal hydrolysis of $RuCl_3$ in the presence of GO and a subsequent phosphidation process,[94] outperforming the activity and stability after 10 h of operation or 1000 cycles of those of Pt/C both at acidic and basic pH. They thus obtained some of the best values reported so far for HER catalysis in 0.5 M H_2SO_4 ($\eta_0 \approx 0$ mV, η_{10} = 22 mV, Tafel slope = 29 mV·dec^{-1} and $|j_0|$= 2.2 mA·cm^{-2}; Table 3, entry 11) and in 1 M KOH ($\eta_0 \approx 0$ mV, η_{10} = 13 mV; Table 4, entry 9). Contrasting to the huge majority of HER nanoparticulated catalysts based on noble metals, whose activity decreases at basic pH vs. acidic pH due to an increase in the hydrophobicity of the metal surface that hampers water adsorption,[96] Ru_2P/RGO shows lower η_{10} values under alkaline conditions than under acidic conditions. According to DFT calculations partial electron transfer from Ru_2P to the surface sp^2 C of RGO favors water dissociation and the subsequent hydrogen adsorption and recombination.[94] In the second recent work, even more active Ru_2P NPs at acidic pH have been obtained after calcination at 900 °C of polyaniline fibers on C cloth with a $RuCl_3 \cdot 3H_2O$, yielding Ru_2P NPs partially encapsulated by a C layer and deposited on top of P/N-doped C nanofibers on C cloth (Ru_2P@PNC/CC-900; Table 3, entry 12, Table 4, entry 10). The superior HER performance is associated to the modification of ΔG_H^* of Ru_2P by the P/N-doped C surface, which boosts their proton adsorption and reduction capacities.[95] Finally, although not being a supported composite system, extremely active and stable (200 h at 10 mA·cm^{-1}) 32 nm RuP NP agglomerates on C (RuP/C, Table 3, entry 10; Table 4, entry 8) have been described both at acidic and basic pH, with higher $|j_0|$ and TOF and lower η_{10} and Tafel slopes than 20% Pt/C at pH 14 and comparable values at pH 0. Curiously, the agglomerates show superior performance and stability than lower size NPs of 3 nm due to better stabilization of the P species for the former thanks to lowered surface energy of larger NPs.[97]

To summarize, the best performing supported Ru NP catalytic systems are composite materials prepared by two different pathways. First, the direct anchoring of a Ru precursor onto a carbon-based electrode followed by an annealing step that allows to form the Ru NPs onto the electrode; second, the

condensation of organic precursors that direct the growth of Ru NPs followed by a carbonization process to form a conductive carbon matrix around the NPs. In these works, it has been proven the catalytic advantages for HER of N-doped C-based supports that lead to increased stability and activity. Also, the appropriate values of the H/H_2O adsorption energy and H_2O dissociation rate onto Ru NPs (especially in their fcc-phase for alkaline HER) and RuP_x NPs together with their long-term stability, have shown the real potentiality of Ru in replacing Pt from WS electrochemical cells in the near future. However, while the carbon matrices where Ru NPs are embedded dramatically affect their catalytic behavior, they do not permit the easy tuning of their active sites, thus challenging the rational improvement of their catalytic performance through the establishment of structure-activity relationships.

4.3. Supported electrochemical systems on metal/semimetal-based materials.

Besides C-based supports, metal or semimetal-based materials such as MoS_2,[98] MoO_2,[99] TiO_2,[100] W,[101] Si,[102] Te,[103] $Y(OH)_3$[104] or CeO_2[105] have also been used as supports. For example, Qiao *et al.* described an extremely active catalyst in basic conditions (1 M KOH).[98] This system involves 10 nm Ru NPs deposited onto MoS_2 nanosheets lying onto carbon paper ($Ru/MoS_2/CP$) obtained by $Ru(OH)_3$ calcination. It achieves $\eta_0 \approx 0$ mV and η_{10} = 13 mV, and is totally stable for 12 h or 1000 cycles (Table 4, entry 22). Interestingly, the HER activity is significantly higher at basic pH than at acidic pH. This results from the fact that at basic conditions the water dissociation process on Ru is coupled with the hydrogen atom adsorption on MoS_2, thus providing a synergistic effect between the Ru NPs and the support. Also, a Ru-MoO_2 composite made of Ru NPs anchored onto 600 nm MoO_2 particles (prepared by $RuCl_3$ pyrolysis onto a suspension of a Mo-based metal organic framework) showed a very high HER activity at basic pH.[99] This catalyst surpassed the Pt/C activity at pH 14 with η_0 = 0 mV, η_{10} = 29 mV and a Tafel slope = 31 $mV \cdot dec^{-1}$ (Table 4, entry 23). From DFT calculations and XPS data, the authors propose that the combination of the weak H binding strength on MoO_2 with the fast electron transfer between Ru and MoO_2 might explain the enhanced HER activity of this nanocomposite both at basic and acidic pH. Similarly, DFT data evidenced that the electronic interaction between Ru and W in a composite nanomaterial made of Ru NPs (2-5 nm) supported on carbon, dispersed into C Black and deposited onto W NPs (60-80 nm) by simple physical mixing (W+Ru/C) led to a diminution of the H binding energy to Ru, thus improving the HER efficiency at acidic pH, reaching comparable activity and higher long-term stability than Pt/C (Table 3, entry 24).[101]

Remarkably, Ru NPs have also been combined/alloyed with Co,[106,107] Ni,[108] NiCo[109] and NiCoMo[110] nanostructures to form heterometallic electrocatalysts showing synergistic effects in HER similar to those above-mentioned for metal/semimetal-based supports. Thus, for example, Su, Yang and co-workers reported the doping of Co-based nanocubes with 3.58 wt.% Ru followed by annealing at high temperature (600 ^oC), which afforded 30 nm in size RuCo nanoalloys encapsulated into N-doped graphene shells (RuCo@NC) of high activity ($\eta_0 \approx 0$ mV, η_{10} = 28 mV, Tafel slope = 31 $mV \cdot dec^{-1}$, $|j_0|$ = 3.31 $mA \cdot cm^{-2}$, Table 4, entry 20) and stability (increase of η_{10} of only 4 mV after 10000 cycles).[106] According to DFT modelling, the presence of Ru increases the electron-transfer from the metallic core to the carbon shell, which lowers the H adsorption energy and increases the HER kinetics. Similarly, Dai and co-workers recently reported the combination of Ru NPs with Ni@Ni_2P nanorods (Ru-Ni@Ni_2P-HNRs), which promoted, compared to the parent Ni_2P system, faster H_2 desorption (optimal H adsorption energy) and a faster electron-transfer, thus enhancing the HER kinetics of the system both at acidic and basic pH (Table 3, entry 28; Table 4, entry 29).[109]

In conclusion, the interaction of metallic Ru with other metal/semimetal-based nanostructures into mixed catalysts has been known to increase the HER catalytic activity compared to that of the respective separated systems as the result of a synergistic effect between both metals, which improves the electron conductivity and lowers the H adsorption energy.

4.4. Photochemical systems.

The inclusion of Ru NPs in HER photocatalytic systems is not an obvious task given the inherent difficulty in properly transferring electrons from a photosensitive molecule or material to the nanocatalyst while avoiding at the same time undesired back-electron transfer processes. Indeed, the electron transfer process between Ru NPs and the widely employed molecular photosensitizer $[Ru(bpy)_3]^{2+}$ is generally not optimal.[111] Thus, together with a sacrificial electron-donor (SED, e.g. NADH) supplying the needed electrons in half-cell systems, the use of an electron mediator (e.g. methyl viologen) is generally necessary. Only PSs attaining sufficient long-lived charge-separated states after photoexcitation are able to inject electrons to the HER electrocatalyst without the need of using an electron mediator, thus making the systems less complex and more efficient.

In this regard, a molecular dyad that acts both as a PS and as an efficient electron supplier for Ru NPs has been described by Fukuzumi and co-workers,[112] the 2-phenyl-4-(1-naphthyl)-quinolinium ion ($QuPh^+$-NA, see Scheme 1). Thus, they studied the photocatalytic HER using PVP-stabilized Ru NPs (PVP = polyvinylpyrrolidone) as catalyst and found optimal conditions for this system using the $QuPh^+$-NA PS in alkaline solution.[112, 113, 114] Two main conclusions can be extracted from their results. First, that there is no increase on the photocatalytic activity above a certain optimal catalyst concentration presumably due to light dispersion and opacity when more nanomaterial is present in the reaction medium. Second, that there is an activity-size dependency of the tested NPs. Small NPs present higher negative charge density, easing the proton reduction process but hindering the hydrogen-atom association step, since there is low density of H atoms on a single particle. Larger NPs ease the hydrogen-atom association step due to the presence of more H atoms on the NP surface, but hinder the previous proton reduction process as the negative charge density of the surface

is initially lower. In consequence, the best results in their study were obtained with NPs of intermediate size, namely 4.1 nm.[112] Besides the $QuPh^+$-NA ion, only the dye Eosin Y[115] and the combination of $[Ru(bpy)_3]^{2+}$ with 9-phenyl-10-methyl-acridinium derivatives as electron mediators[116] have led to relative success in the photocatalytic HER with Ru-based NPs.

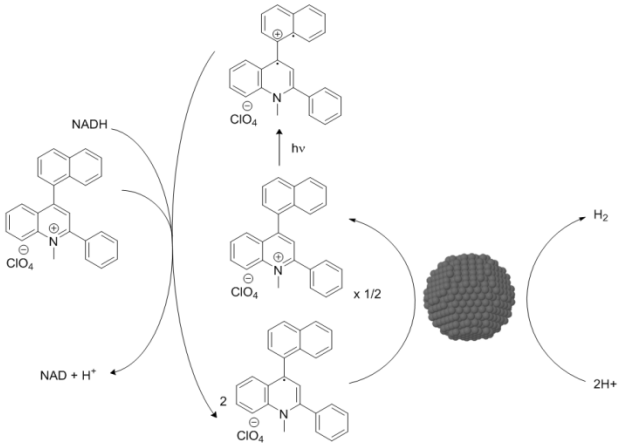

Scheme 1. Schematic representation of the electron transfer processes involved in photocatalytic hydrogen evolution promoted by Ru NPs in the presence of the $QuPh^+$-NA organic donor-acceptor photoabsorber described by Fukuzumi et al. Adapted from ref. [112].

Still in the presence of $QuPh^+$-NA as PS, the use of oxide-based materials (SiO_2, TiO_2, CeO_2, etc.) as supports for the Ru NPs led to less agglomeration under HER turnover conditions and, consequently, to enhanced photocatalytic stability with regards to the corresponding non-supported systems.[111] In a similar direction but replacing the molecular PS by an organic bulk heterojunction layer able to absorb light and drive photoinduced exciton separation, organic photocathodes bearing RuO_2 NPs as catalytic centres yielded high photovoltages and photocurrent densities, as recently reported by Francàs, Durrant and co-workers.[117] Finally, Ru NPs have been recently included as HER co-catalysts in tandem particle overall water splitting photocatalysts (Ru-$SrTIO_3$:Ru/$BiVO_4$[118] and doped derivatives[119]). Even if still at its infancy in terms of development, tandem particle-based photocatalysts are promising candidates with theoretically high limiting efficiency (*ca.* 28%) and relatively low fabrication costs.

Table 3. Comparison of the most relevant Ru-based HER nanoelectrocatalysts under acidic conditions. Parameters: mean diameter (Ø), onset overpotential (η_0, mV), overpotential at $|j|$ =10 mA·cm^{-2} (η_{10}, mV), Tafel slope (b, mV·dec^{-1}), exchange current density ($|j_0|$, mA·cm^{-2}), specific current density ($|j_S|$, mA·cm^{-2}) and turnover frequency (TOF, s^{-1}). Unless otherwise stated, electrolyte is 0.5 M H_2SO_4.

Entry	Catalyst	Ø (nm)	η_0 (mV)	η_{10} (mV)	b (mV·dec^{-1})	$\|j_0\|$ (mA·cm^{-2})	$\|j_S\|$ (mA·cm^{-2})	TOF (s^{-1})	Ref.
1	RuO_2-C (Vulcan)	5-8	≈ 0	≈ 15	26	-	-	-	64
2	GCE-S-GNs-1000-CB-Ru	30	≈ 60	80	61 (Tafel) 71 (EIS)	0.541 0.431	-	-	69
3	Ru-GC	100	10	90	≈ 33	-	-	-	71
4	Ru-GLC	2-5	3	35	46	-	-	-	83
5	RuO_2-NWs@g-CN	10-40	14	93	40	0.22	-	-	38
6	Ru/g-C_3N_4/C	2	≈ 15-20	≈ 70	-	-	-	≈ 4.85 (100 mV)	88
7	Ru@C_2N	1.6	9.5	22 (13.5 after 1000 cycles)	30	1.9	-	0.67 (25 mV) 1.95 (50 mV)	15
8	Ru-CCS	3.25 ± 0.73	11.0	27.3	33	-	-	3.70 (50 mV)	90
9	RuP_x@NPC	4	25	51	46	-	-	-	92
10	RuP/C	32	≈ 0	19	37	3.22	-	3.35 (20 mV)	97
11	Ru_2P/RGO	<7	≈ 0	22	29	2.2	-	-	94
12	Ru_2P@PNC/CC-900	20.19 ± 9.62	≈ 0	15	28	-	-	-	95
13	RuP_2@NPC	8	≈ 0	38	38	1.99	-	-	93
14	Ru@CN	2.37	≈ 70	126	-	-	-	-	84
15	Ru-NGC	≈ 5	9.5	25	31	-	-	0.68 (30 mV)	79
16	Ru@GnP	2	≈ 0	13	30	-	-	0.26 (100 mV)	81
17	Ru-HPC	2.87	≈ 15	61.6	66.8	1.2	-	0.18 (25 mV)	40
18	Ru/CeO_2	3.89 ± 1.24	33	47	41	0.67	-	0.8 (27 mV)	105
19	Ru-GC (Ru-MeOH/THF)	21.4	0	83	46	-	0.36 (100 mV)	0.07 (25 mV) 0.10 (50 mV) 0.87 (100 mV)	73
20	Ru/MoS_2/CP	10	≈ 60	96	-	-	-	-	98
21	Ru-MoO_2	-	≈ 0	55	44	-	-	-	99
22	Ru(0)/TiO_2	4.7 ± 1.2	34	41	52	0.728	-	-	100
23	$Ni_{1.5}Co_{1.4}P$@Ru	4	≈ 0	49	49	1.26	-	-	108
24	W+Ru/C	2-5	≈ 45	85	46	0.049	-	-	101

25	PP-Ru-GC [a]	1.5 ± 0.3	0	20	29	-	0.55 (100 mV)		0.55 (25 mV) 3.06 (50 mV) 17.38 (100 mV)	74
26	Te@Ru	-	≈ 40	86	36	-	0.14 (86 mV)		0.82 (100 mV)	103
27	CoRu@NC	10-30	≈ 7	32	47	-	-		-	107
28	Ru-Ni@Ni_2P-HNRs	4.71	≈ 20	51	35	0.32	-		0.78 (10 mV) 0.88 (20 mV) 1.10 (100 mV)	109
29	0.27-RuO_2@C	5	≈ 0	33	53	-	-			33
30	hcp-Ru@NC-700	4	≈ 0	27.5	37	-	-		1.6 (25 mV)	65

Electrolyte: [a] 1 M H_2SO_4.

Table 4. Comparison of the most relevant Ru-based HER nanoelectrocatalysts under basic conditions. Parameters: mean diameter (Ø), onset overpotential (η_0, mV), overpotential at $|j|$ =10 mA·cm^{-2} (η_{10}, mV), Tafel slope (b, mV·dec^{-1}), exchange current density ($|j_0|$, mA·cm^{-2}), specific current density ($|j_S|$, mA·cm^{-2}) and turnover frequency (TOF, s^{-1}). Unless otherwise stated, electrolyte is 1.0 M KOH/NaOH.

Entry	Catalyst	Ø (nm)	η_0 (mV)	η_{10} (mV)	b (mV·dec^{-1})	$\|j_0\|$ (mA·cm^{-2})	$\|j_S\|$ (mA·cm^{-2})	TOF (s^{-1})	Ref.
1	RuO_2-NWs@g-CN [b]	10-40	16	95	70	0.28	-	-	38
2	Ru@C_2N	1.6	-	17	38	-	-	0.76 (25 mV) 1.66 (50 mV)	15
3	hydrous-RuO_2	< 5	≈ 25	60	-	-	-	-	29
4	crystalline-RuO_2	-	≈ 25	74	-	-	-	-	29
5	Ru/g-C_3N_4/C [a]	2	≈ 15-20	79	-	0.46	-	4.2 (100 mV)	88
6	Ru/NG-750	5.8 ± 1.5	0	8	30	-	-	0.35 (100 mV)	66
7	RuP_x@NPC	4	≈ 30	74	70	-	-	-	92
8	RuP/C	32	≈ 0	18	34	3.07	-	3.62 (20 mV)	97
9	Ru_2P/RGO	<7	≈ 0	13	56	-	-	-	94
10	Ru_2P@PNC/CC-900	20.19 ± 9.62	≈ 25	50	66	-	-	-	95
11	RuP_2@NPC	8	≈ 0	52	69	-	-	-	93
12	Ru@CN	2.37	≈ 0	32	53	-	-	-	84
13	Ru@NC	1.6	15	26	36	-	-	0.83 (25 mV) 3.02 (50 mV) 10.8 (100 mV)	82
14	Ru/CN-800	≈ 1.3	≈ 0	14	30.0	-	-	-	77
15	Ru/3DNPC-500	1.32	≈ 0	15	31	-	-	-	78

16	Ru-NGC	≈ 5	≈ 12.5	≈ 37	40	-	-	-	79
17	CN_x@Ru/MWCNT	6.0 ± 2.3	20	39	28	-	-	-	80
18	Ru@GnP	2	≈ 0	22	28	-	-	0.145 (100 mV)	81
19	Ru-HPC	2.87	≈ 0	≈ 5	33.9	6.59	-	1.79 (25 mV) 9.2 (100 mV)	40
20	RuCo@NC	30	≈ 0	28	31	3.31	-	-	106
21	CoRu@NC	10-30	≈ 20	45	66	-	-	-	107
22	Ru/MoS_2/CP	10	≈ 0	13	60	-	0.075 (50 mV)	-	98
23	Ru-MoO_2	-	0	29	31	-	-	-	99
24	$Ni_{1.5}Co_{1.4}P$@Ru	4	≈ 12	52	50	-	-	-	108
25	Ru/C-300	1.48	≈ 0	14	32.5	-	-	-	67
26	PP-Ru/RuO_2-GC	1.5 ± 0.3	0	25	65	-	0.19 (100 mV)	-	74
27	Ru/C	1.73 ± 0.47	≈ 0	24	33	-	-	0.18 (40 mV)	76
28	Cu-doped Ru-RuO_2/C	2.5-4.5	≈ 15	28	35	-	-	-	47
29	Ru-Ni@Ni_2P-HNRs	4.71	≈ 5	31	41	-	-	-	109
30	NiCoMo/Ru-GN [a]	-	≈ 0	11.4	38	6.31	-	-	110
31	0.27-RuO_2@C	5	≈ 0	20	46	-	-	-	33
32	ah-RuO_2@C	150	≈ 20	63	62	-	-	-	33

Electrolyte: [a] 0.1 M KOH and [b] 0.5 M KOH.

5. Bifunctional Ru/RuO_2 systems and their use in WS electrolytic cells

As noted above in Sections 3 and 4, Ru-based nanoparticulated materials are good candidates for acting either as anodes (OER) or as cathodes (HER) in WS electrocatalytic cells. Furthermore, some studies have revealed the ability of Ru NPs to act both as OER and HER electrocatalysts, thus becoming real bifunctional catalysts after a slight modification of their structure/oxidation state or even without any further change. This section accounts on such bifunctional electrocatalysts and, when reported, on their implementation in overall WS electrolytic cells.

Given the instability (corrosion) of metallic Ru NPs under OER conditions[31] (typically overoxidized to molecular RuO_4, see Section 3.1 above), bifunctional Ru-based nanoparticulated systems are typically RuO_2 or Ru/RuO_2 mixtures. Besides catalyzing the OER, RuO_2 has also been reported as a HER electrocatalyst. As established by recent works,[63,74] this suggests a change of the oxidation state at its surface due to the reductive conditions applied (see Section 4.1 above), which may favor the formation of a Ru-H bond. However, the evolution of the Ru oxidation state at the surface of the NPs under HER conditions is not always monitored, and the reports only consider the original composition of the catalyst.

A first set of Ru-based electrolyzers for the whole WS deals with the use of RuO_2 NPs both in the anode and in the cathode. For instance, Lim and co-workers reported a hydrous/crystalline RuO_2 bifunctional electrocatalyst and its integration in an efficient cell for the overall splitting of water. These authors reported the combination of a cathode made of stable hydrous RuO_2 NPs/Ni foam (Table 4, entry 3) with a crystalline-RuO_2/Ni foam anode obtained by annealing the former hydrous species (Table 2, entry 3). This combination of electrodes afforded an efficient alkaline electrolyzer, achieving an overall $\eta_0 \approx 170$ mV and $\eta_{10} = 273$ mV, values that outperform those obtained with (Pt/C)/Ni and IrO_2/Ni as cathodic and anodic electrode materials, respectively.[29] In a related example, Jang, Song and co-workers recently described the use of partially hydrous RuO_2 NPs embedded in a C matrix as a multifunctional electrocatalyst,[33] being the HER (Table 3, entry 29; Table 4, entry 31) and the OER (Table 1, entry 7; Table 2, entry 8) two of its functionalities (see Sections 3 and 4 for more details). When used both as cathode and anode in a WS electrocatalytic cell at pH 14, this nanomaterial yields and overall η_{10} of 280 mV. This result also highlights the potential of the *alternating* operation mode of their electrolyzer by switching the employed HER/OER electrodes, thus demonstrating a superior durability of the system since long-term exposure to oxidative (or reductive) environments is avoided. Also, Barman *et al.* published a bifunctional catalyst made of crystalline rutile RuO_2-nanowires (100-200 nm in length and 10-40 nm in diameter) supported onto carbon nitride (RuO_2-NWs@g-CN),[38] able to catalyze both the OER (Table 1, entry 3; Table 2, entry 4) and the HER (Table 3, entry 5; Table 4, entry 1) with good-to-moderate activities and high stabilities at acidic and basic pH. Moreover, when used in both the cathode and the anode of a WS electrolytic cell at pH 14 this nanomaterial afforded an overall $\eta_0 \approx 100$ mV and $\eta_{10} = 300$ mV.

A second set of Ru-based WS electrolyzers are those combining metallic Ru and RuO_2 either as pure or as mixed electrode materials. Thus, Chen and co-workers have recently described the bifunctional catalytic character of a Cu-doped Ru-RuO_2/C composite (Table 2, entry 5; Table 4, entry 28),[47] in which a mixture of 2.5-4.5 nm fcc and hcp-Ru NPs and rutile-RuO_2 NPs doped with Cu are embedded in a C matrix. They assigned the HER activity of the material to the Ru NPs, and the OER one to the RuO_2 NPs. When using this composite material in both the cathode and the anode of a WS electrolytic cell at pH 14 an overall η_{10} of 240 mV is achieved. Finally, a second relevant example of such a type of electrolyzers has been recently reported by Zou and co-workers[40] arising from the combination of their Ru-HPC/P-RuO_2 hierarchical cathodic/anodic materials (see Sections 3.3.1 and 4.2 for the description of the individual performance in OER and HER, respectively) that originate from the pyrolytic decomposition of a CuRu-MOF. The two-electrode WS device operates at an overall η_{10} of 300 mV in 1.0 M KOH and shows excellent long-term (24 h) stability at a cell voltage of 1.65 V.

6. Conclusions and Challenges

In the last decade Ru-based NPs have clearly emerged as practical (electro)catalytic systems for the two half-cell reactions in water splitting. In this regard, benchmarking methodologies, which have become widespread along the same period, have objectively shown the comparable or occasionally even superior performance of Ru-based NP systems to the standard Pt and IrO_x species used for catalyzing the HER and the OER in commercial electrolyzers, respectively. At the same time, the fair comparison of catalysts through benchmarking strategies has also allowed to identify the main drawbacks characterizing these systems.

A quick glance at the primary figures of merit for the most representative HER and OER electrocatalysts (particularly η_{10}, Tafel slope (b) and TOF per real active site) highlights the divergence in mechanistic complexity of the two half-reactions. Thus, HER systems show clearly faster kinetics (TOFs about one order of magnitude higher, compare Figures 3 and 6) and attain practical current densities (η_{10}) at much lower overpotentials (below 100 mV for the HER, Figure 5, and above 200 mV for the OER, Figure 2).

OER catalysts work in harsh oxidative conditions that usually compromise their stability. This is the case of metallic Ru NPs (and certain Ru/RuO_2 mixtures), which tend to over-oxidize to the soluble and volatile RuO_4 form under turnover conditions. Though, pure RuO_2 or core-shell systems where a Ru shell is combined with a more noble metal core tend to be more stable. Thus, even if the main activity-related figures of merit for Ru-based nanoparticulated OER electrocatalysts (see Tables 1 and 2) are comparable to those of the state-of-the-art IrO_x species, strategies to rationally improve their long-term stability must be

further developed. Together, the influence of the degree of crystallinity of the nanocatalysts both in terms of activity and stability is another unclear matter, currently with non-conclusive and even contradictory reports. Also, supported Ru NP-based OER systems are relatively scarce and have been mainly developed with SiO_2 materials of different porosity and pore size while triggered both chemically and/or photochemically. Together with the general effect of the support preventing NP aggregation under turnover conditions and thus improving the catalyst durability, pores large enough to ensure both the proper exposure of the NP active sites and the correct diffusion of the oxidants/photoabsorbers used have proven to be a key feature of these systems. All in all, the establishment of structure-activity/stability relationships remains as the main challenge in the OER field when employing Ru NPs as catalysts. In this regard, the combination of advanced (and operando) NP surface characterization techniques and computational modelling appears as a promising track still almost unexplored today.

As stated in Section 4, the development of Ru-based NPs as catalysts for the HER is a dynamic field of research where many advances have been made in the last three years. Contrary to the OER, the majority of Ru-based NPs systems reported for the HER are electrocatalysts that have been benchmarked through the typical figures of merit discussed in Section 2 (see Tables 3 and 4) and their mechanistic pathways have been related to structural/electronic features of the NPs or NP-based hybrids by combining both experimental and theoretical DFT calculations. As stated above, the distinction between "non-supported" (Section 4.1) and "supported" (Section 4.2) systems is of interest. The formers are simpler systems where the active sites of the NPs can be tuned with ease and the surface chemistry resembles somehow that of molecular complexes. In this regard, the organometallic approach for the synthesis of nanostructures (see above) opens a myriad of possibilities by means of the inexhaustible ligand pool of NP stabilizers. The combination of electrochemical analysis, detailed structural and surface characterization and DFT modelling of the involved reaction pathways can lead to structure-activity/stability relationships, thus allowing the subsequent rational improvement of the electrocatalytic HER systems. In contrast, the "supported" systems are more complex hybrid or composite materials of difficult tunability, where the interaction of the Ru NPs with the typically carbon-based support/matrix results on increased stability (aggregation is prevented) and, in some cases, on particularly interesting catalytic properties arising from the support/matrix influence on the catalysts structure. Thus, for instance, these systems have shown appropriate H/H_2O adsorption energies and H_2O dissociation rates in alkaline solution (especially when Ru adopts its uncommon fcc-phase) that, together with their long-term stability at this pH, have raised Ru-based nanoparticulated electrocatalysts as plausible candidates to replace Pt in cathodes for practical WS. However, most of the above-mentioned systems are complex and/or of difficult scalability, and very few have been triggered by light. Thus, the development of simple, scalable and cost-effective HER electrocatalytic systems based on Ru NPs and their triggering by sunlight in combination with molecular or semiconducting photoabsorbers are two of the main challenges the field will face in the upcoming years.

The deep mechanistic understanding attained in the last decade for Ru molecular complexes can also serve as a reservoir of inspiration to develop improved HER and OER nanomaterials. Thus, the potential benefits of transferring key molecular concepts such as, for instance, the kinetic effects of internal bases, the redox-activity of capping molecules/ligands or the fine-tuning of redox potentials should be carefully assessed. Again, combination of experimental and computational analyses will be imperative in this complex endeavor.

Finally, a very encouraging field has been opened lately with the use of real bifunctional HER/OER Ru-based NPs. Thus, as stated in Section 5, the use of either RuO_2 or the combination of metallic Ru and RuO_2, either as pure or as mixed electrode materials, has been reported and, even more importantly, these materials have been successfully incorporated into compact water splitting electrocatalytic cells.

Acknowledgements

Sustained support from MINECO, FEDER, AGAUR, CNRS, the University Paul Sabatier – Toulouse and the GDRI HC3A Franco-Catalan action are gratefully acknowledged. Recent research projects and grants include CTQ2011-26440, CTQ2015-64261-R, IDEX UNITI Emergence project (UFTMIP: 2015-209-CIF-D-DRD-127185), CTP2013-0016 and Midi-Pyrénées/n°13053026. J.C. thanks the UAB and the "Euroregió Pirineus Mediterrània" for predoctoral grants. J. De T. acknowledges the UAB for a PIF predoctoral grant. J.G.-A. acknowledges the Serra Húnter Program.

Keywords: ruthenium • nanoparticle • hydrogen evolution reaction • oxygen evolution reaction • electrocatalysis

Entry for the Table of Contents

REVIEW

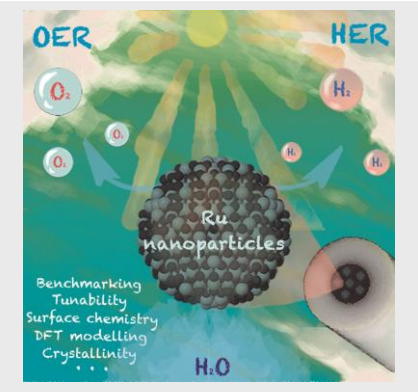

HER and OER catalysts are key components for obtaining new sustainable energy conversion schemes based on water splitting and sunlight. This review covers the most significant developments on Ru-based nanoparticles as catalysts for these processes, focusing on the factors governing their performance.

J. Creus, J. De Tovar, N. Romero, J. García-Antón, K. Philippot, R. Bofill*, and X. Sala**

Page No. – Page No.

Ruthenium Nanoparticles for Catalytic Water Splitting

[1] L. N. Lewis, *Science* **2016**, *351*, 6271.

[2] C. Amiens, B. Chaudret, D. Ciuculescu-Pradines, V. Collière, K. Fajerwerg, P. Fau, M. Kahn, A. Maisonnat, K. Philippot, *New J. Chem.* **2013**, *37*, 3374-3401.

[3] C. J. Murphy, J. M. Buriak, *Chem. Mater.* **2015**, *27*, 4911-4913.

[4] C. C. L. McCrory, S. Jung, J. C. Peters, T. F. Jaramillo, *J. Am. Chem. Soc.* **2013**, *135*, 16977-16987.

[5] A. Harriman, I. J. Pickering, J. M. Thomas, P. A. Christensen, *J. Chem. Soc., Faraday Trans. 1* **1988**, *84*, 2795-2806.

[6] H. Over, *Chem. Rev.* **2012**, *112*, 3356-3426.

[7] I. C. Man, H.-Y. Su, F. Calle-Vallejo, H. A. Hansen, J. I. Martínez, N. G. Inoglu, J. Kitchin, T. F. Jaramillo, J. K. Nørskov, J. Rossmeisl, *ChemCatChem* **2011**, *3*, 1159-1165.

[8] E. A. Paoli, F. Masini, R. Frydenal, D. Deiana, C. Schlaup, M. Malizia, T. W. Hansen, S. Horch, I. E. L. Stephens, I. Chorkendorff, *Chem. Sci.* **2015**, *6*, 190-196.

[9] X. Sala, S. Maji, R. Bofill, J. García-Antón, L. Escriche, A. Llobet, *Acc. Chem. Res.* **2014**, *47*, 504-516.

[10] R. Matheu, M. Z. Ertem, J. Benet-Buchholz, E. Coronado, V. S. Batista, X. Sala, A. Llobet, *J. Am. Chem. Soc.* **2015**, *137*, 10786-10795.

[11] P. Garrido-Barros, C. Gimbert-Suriñach, R. Matheu, X. Sala, A. Llobet, *Chem. Soc. Rev.* **2017**, *46*, 6088-6098.

[12] R. Matheu, L. Francàs, P. Chernev, M. Z. Ertem, V. Batista, M. Haumann, X. Sala, A. Llobet, *ACS Catal.* **2015**, *5*, 3422-3429.

[13] J. K. Nørskov, T. Bligaard, A. Logadottir, J. R. Kitchin, J. G. Chen, S. Pandelov, U. Stimming, *J. Electrochem. Soc.* **2005**, *152*, J23-J26.

[14] Y. Zheng, Y. Jiao, M. Jaroniec, S.Z. Qiao, *Angew. Chem. Int. Ed.* **2015**, *54*, 52-65.

[15] J. Mahmood, F. Li, S. Jung, M. S. Okyay, I. Ahmad, S. Kim, N. Park, H. Y. Jeong, J. Baek, *Nature Nanotech.* **2017**, *12*, 441-446.

[16] C. C. L. McCrory, S. Jung, I. M. Ferrer, S. M. Chatman, J. C. Peters, T. F. Jaramillo, *J. Am. Chem. Soc.* **2015**, *137*, 4347-4357.

[17] M. P. Browne, C. O'Rourke, N. Wells, A. Mills, *ChemPhotoChem* **2018**, *2*, 293-299.

[18] M. P. Browne, C. O'Rourke, A. Mills, *Electrochem. Commun.* **2017**, *85*, 1-5.

[19] S. Anantharaj, S. R. Ede, K. Karthick, S. S. Sankar, K. Sangeetha, P. E. Karthik, S. Kundu, *Energy Environ. Sci.* **2018**, *11*, 744-771.

[20] S. Jung, C. C. L. McCrory, I. M. Ferrer, J. C. Peters, T. F. Jaramillo, *J. Mater. Chem. A* **2016**, *4*, 3068-3076.

[21] C. Spöri, J. T. H. Kwan, A. Bonakdarpour, D. P. Wilkinson, P. Strasser, *Angew. Chem. Int. Ed.* **2017**, *56*, 5994-6021.

[22] C. Wei, R. R. Rao, J. Peng, B. Huang, I. E. L. Stephens, M. Risch, Z. J. Xu, Y. Shao-Horn, *Adv. Mater.* **2019**, 1806296.

[23] R. L. Doyle, I. J. Godwin, M. P. Brandon, M. E. G. Lyons, *Phys. Chem. Chem. Phys.* **2013**, *15*, 13737-13783.

[24] C. L. Gree, A. Kucernak, *J. Phys. Chem. B* **2002**, *106*, 1036-1047.

[25] T. Shinagawa, A. T. Garcia-Esparza, K. Takanabe, *Sci. Rep.* **2015**, 5:13801.

[26] S. Fletcher, J. Solid State Electrochem. **2009**,*13*, 537-549.

[27] T. Shinagawa, A. T. Garcia-Esparza, K. Takanabe, *Sci. Rep.* **2015**, *5*, Article nº 13801; B. E. Conway, B. V. Tilak, *Electrochim. Acta* **2002**, *47*, 3571-3594.

[28] M. Zeng, Y. Li, *J. Mater. Chem. A* **2015**, *3*, 14942-14962.

[29] J. Lee, S. A. S. Shah, P. J. Yoo, B. Lim, *Chem. Phys. Lett.* **2017**, *673*, 89-92.

[30] K. Maeda, R. Abe, K. Domen, *J. Phys. Chem. C* **2011**, *115*, 3057-3064.

[31] T. Reier, M. Oezaslan, P. Strasser, *ACS Catal.* **2012**, *2*, 1765-1772.

[32] Y. Zhang, T. Ren, *Chem. Commun.* **2012**, *48*, 11005-11007.

[33] H.-S. Park, J. Yang, M. K. Cho, Y. Lee, S. Cho, S.-D. Yim, B.-S. Kim, J. H. Jang, H.-K. Song, *Nano Energy* **2019**, *55*, 49-58.

[34] E. S. Gnanakumar, W. Ng, B. C. Filiz, G. Rothenberg, S. Wang, H. Xu, L. Pastor-Pérez, M. M. Pastor-Blas, A. Sepúlveda-Escribano, N. Yan, N. R. Shiju, *ChemCatChem* **2017**, *9*, 4159-4163.

[35] J. Xu, S. Murphy, D. Xiong, R. Cai, X.-K. Wei, M. Heggen, E. Barborini, S. Vinati, R. E. Dunin-Borkowski, R. E. Palmer, *ACS Appl. Energy Mater.* **2018**, *1*, 3013-3018.

[36] S. Y. Tee, C. J. J. Lee, S. S. Dinachali, S. C. Lai, E. L. Williams, H.-K. Luo, D. Chi, T. S. A. Hor, M.-Y. Han, *Nanotechnology* **2015**, *26*, 415401-415407.

[37] Y. Lee, J. Suntivich, K. J. May, E. E. Perry, Y. Shao-Horn, *J. Phys. Chem. Lett.* **2012**, *3*, 399-404.

[38] T. Bhowmik, M. K. Kundu, S. Barman, *ACS Appl. Mater. Interfaces* **2016**, *8*, 28678-28688.

[39] X. Kong, K. Xu, C. Zhang, J. Dai, S. N. Oliaee, L. Li, X. Zeng, C. Wu, Z. Peng, *ACS Catal.* **2016**, *6*, 1487-1492.

[40] T. Qiu, Z. Liang, W. Guo, S. Gao, C. Qu, H. Tabassum, H. Zhang, B. Zhu , R. Zou, Y. Shao-Horn, *Nano Energy* **2019**, *58*, 1-10.

[41] K. P. J. Gustafson, A. Shatskiy, O. Verho, M. D. Kärkäs, B. Schluschass, C. Tai, B. Åkermark, J. Bäckvall, E. V. Johnston, *Catal. Sci. Technol.* **2017**, *7*, 293-299.

[42] K. Okeyoshi, R. Yoshida, *Adv. Funct. Mater.* **2010**, *20*, 708-714.

[43] H. Yoo, Y. Choi, J. Choi, *ChemCatChem* **2015**, *7*, 643-647.

[44] A. Mills, P. A. Duckmanton, J. Reglinski, *Chem. Commun.* **2010**, *46*, 2397-2398.

[45] S. Stucki, A. Menth, *Ber. Bunsen-Ges.* **1980**, *84*, 1008-1013.

[46] K. A. Stoerzinger, L. Qiao, M. D. Biegalski, Y. Shao-Horn, *J. Phys. Chem. Lett.* **2014**, *5*, 1636-1641.

[47] K. Yang, P. Xu, Z. Lin, Y. Pang, P. Jiang, C. Wang, S. Liu, S. Gong, L. Hu, Q. Chen, *Small* DOI: 10.1002/smll.201803009.

[48] L. Wang, Q. Zhou, Z. Pu, Q. Zhang, X. Mu, H. Jing, S. Liu, C. Chen, S. Mu, *Nano Energy* **2018**, *53*, 270-276.

[49] E. Tsuji, A. Imanishi, F. Fukui, Y. Nakato, *Electrochimica Acta* **2011**, *56*, 2009-2016.

[50] R. Kötz, H. J. Lewerenz, S. Stucki, *J. Electrochem.Soc.* **1983**, *130*, 825-829.

[51] L. Gloag, T. M. Benedetti, S. Cheong, R. F. Webster, C. E. Marjo, J. J. Gooding, R. D. Tilley, *Nanoscale* **2018**, *10*, 15173-15177.

[52] L. Gloag, T. M. Benedetti, S. Cheong, C. E. Marjo, J. J. Gooding, R. D. Tilley, *J. Am. Chem. Soc.* **2018**, *140*, 12760-12764.

[53] L. Gloag, T. M. Benedetti, S. Cheong, Y. Li, X.-H. Chan, L.-M. Lacroix, S. L. Y. Chang, R. Arenal, I. Florea, H. Barron, A. S. Barnard, A. M. Henning, C. Zhao, W. Schumann, J. J. Gooding, R. D. Tilley, *Angew. Chem. Int. Ed.* **2018**, *57*, 10241-10245.

[54] L. Francàs, X. Sala, J. Benet-Buchholz, L. Escriche, A. Llobet, *ChemSusChem* **2009**, *2*, 321-329.

[55] A. C. Sander, A. Schober, S. Dechert, F. Meyer, *Eur. J. Inorg. Chem.* **2015**, *26*, 4348-4353.

[56] B. Radaram, J. A. Ivie, W. M. Singh, R. M. Grudzient, J. H. Reibenspies, C. E. Webster, X. Zhao, *Inorg. Chem.* **2011**, *50*, 10564-10571.

[57] X. Elias, Q. Liu, C. Gimbert-Suriñach, R. Matheu, P. Mantilla-Perez, A. Martinez-Otero, X. Sala, J. Martorell, A. Llobet, *ACS Catal.* **2016**, 6, 3310-3316.

[58] N. C. King, C. Dickinson, W. Zhou, D. W. Bruce, *Dalton Trans.* **2005**, *6*, 1027-1032.

[59] M. Roca-Ayats, E. Herreros, G. García, M. A. Peña, M. V. Martínez-Huerta, *Appl. Catal. B Environ.* **2016**, *183*, 53-60.

[60] E. Demir, S. Akbayrak, A. M. Önal, S. Özkar, *J. Colloid Interface Sci.* **2019**, *534*, 704-710.

[61] Y. Zhang, E. C. Judkins, D.R. McMillin, D. Mehta, T. Ren, *ACS Catal.* **2013**, *3*, 2474-2478.

[62] T. E. Lister, Y. V. Tolmachev, Y. Chu, W. G. Cullen, H. You, R. Yonco, Z. Nagy, *J. Electroanal. Chem.* **2003**, *554/555*, 71-76.

[63] L. A. Näslund, A. S. Ingason, S. Holmin, J. Rosen, *J. Phys. Chem. C* **2014**, *118*, 15315-15323.

[64] J. Cheng, H. Zhang, H. Ma, H. Zhang, Y. Zou, *Electrochim. Acta* **2010**, *55*, 1855-1861.

[65] Y. Li, L. A. Zhang, Y. Qin, F. Chu, Y. Kong, Y. Tao, Y. Li, Y. Bu, D. Ding, M. Liu, *ACS Catal.* **2018**, 8, 5714-5720.

[66] R. Ye, Y. Liu, Z. Peng, T. Wang, A. S. Jalilov, B. I. Yakobson, S. H. Wei, J. M. Tour, *ACS Appl. Mater. Interfaces* **2017**, *9*, 3785-3791.

[67] C. Xu, M. Ming, Q. Wang, C. Yang, G. Fan, Y. Wan, D. Gao, J. Bi, Y. Zhang, *J. Mater. Chem. A* **2018**, *6*, 14380-14386.

[68] G. Rahman, S. A. Mian, A. H. A. Shah, O. S. Joo, *J. Appl. Electrochem.* **2016**, *46*, 459-468.

[69] R. K. Shervedani, A. Amini, *Carbon* **2015**, *93*, 762-773.

[70] Y. Sugawara, K. Kamata, T. Yamaguchi, *ACS Appl. Energy Mater.* **2019**, *2*, 956-960

[71] K. Magdić, K. Kvastek, V. Horvat-Radošević, *Electrochim. Acta* **2015**, *167*, 455-469.

[72] C. Amiens, D. Ciuculescu-Pradines, K. Philippot, *Coord. Chem. Rev.* **2016**, *308*, 409-432.

[73] S. Drouet, J. Creus, V. Collière, C. Amiens, J. García-Antón, X. Sala, K. Philippot, *Chem. Commun.* **2017**, *53*, 11713-11716.

[74] J. Creus, S. Drouet, S. Suriñach, P. Lecante, V. Collière, R. Poteau, K. Philippot, J. García-Antón, X. Sala, *ACS Catal.* **2018**, 8, 11094-11102.

[75] J. Creus, L. Mallón, N. Romero, R. Bofill, A. Moya, J. L. G. Fierro, R. Mas-Ballesté, X. Sala, K. Philippot, J. García-Antón, *Eur. J. Inorg. Chem.* DOI: 10.1002/ejic.201801438.

[76] Q. Wang, M. Ming, S. Niu, Y. Zhang, G. Fan, J.-S. Hu, *Adv. Energy Mater.* **2018**, *8*, 1801698.

[77] X. Cheng, H. Wang, M. Ming, W. Luo, Y. Wang, Y. Yang, Y. Zhang, D. Gao, J. Bi, G. Fan, *ACS Sustainable Chem. Eng.* **2018**, *6*, 11487-11492.

[78] H. Wang, C. Xu, Q. Chen, M. Ming, Y. Wang, T. Sun, Y. Zhang, D. Gao, J. Bi, G. Fan, *ACS Sustainable Chem. Eng.* **2019**, *7*, 1178-1184.

[79] Q. Song, X. Qiao, L. Liu, Z. Xue, C. Huang, T. Wang, *ChemComm* **2019**, *55*, 965-968.

[80] W. Gou, J. Li, W. Gao, Z. Xia, S. Zhang, Y. Ma, *ChemCatChem* **2019** DOI: 10.1002/cctc.201900006.

[81] F. Li, G.-F. Han, H.-J. Noh, I. Ahmad, I.-Y. Jeon, J.-B. Baek, *Adv. Mater.* **2018**, *30*, 1803676.

[82] Z. L. Wang, K. Sun, J. Henzie, X. Hao, C. Li, T. Takei, Y. M. Kang, Y. Yamauchi, *Angew. Chem. Int. Ed.* **2018**, *57*, 5848-5852.

[83] Z. Chen, J. Lu, Y. Ai, Y. Ji, T. Adschiri, L. Wan, *ACS Appl. Mater. Interfaces* **2016**, *8*, 35132-35137.

[84] J. Wang, Z. Wei, S. Mao, H. Li, Y. Wang, *Energy Environ. Sci.* **2018**, *11*, 800-806.

[85] X. Zhang, A. Chen, Z. Zhang, M. Jiao, Z. Zhou, *J. Mater. Chem. A* **2018**, *6*, 11446-11452.

[86] J. Zhang, P. Liu, G. Wang, P. P. Zhang, X. D. Zhuang, M. W. Chen, I. M. Weidinger, X. L. Feng, *J. Mater. Chem. A* **2017**, *5*, 25314-25318.

[87] B. Lu, L. Guo, F.Wu, Y. Peng, J. E. Lu, T. J. Smart, N. Wang, Y. Z. Finfrock, D. Morris, P. Zhang, N. Li, P. Gao, Y. Ping, S. Chen, *Nat. Commun.* **2019**, *10*, 631.

[88] Y. Zheng, Y. Jiao, Y. Zhu, L. H. Li, Y. Han, M. Jaroniec, S.-Z. Qiao, *J. Am. Chem. Soc.* **2016**, *138*, 16174-16181.

[89] K. Gao, Y. Wang, Z. Wang, Z. Zhu, J. Wang, Z. Luo, C. Zhang, X. Huang, H. Zhang, W. Huang, *Chem. Commun.* **2018**, *54*, 4613-4616.

[90] D. Luo, B. Zhou, Z. Li, X. Qin, Y. Wen, D. Shi, Q. Lu, M. Yang, H. Zhou, Y. Liu, *J. Mater. Chem. A* **2018**, *6*, 2311-2317.

[91] Y. Shi, B. Zhang, *Chem. Soc. Rev.* **2016**, *45*, 1529-1541.

[92] J. Q. Chi, W. K. Gao, J. H. Lin, B. Dong, K. L. Yan, J. F. Qin, B. Liu, Y. M. Chai, C. G. Liu, *ChemsusChem* **2018**, *11*, 743-752.

[93] Z. Pu, I. S. Amiinu, Z. Kou, W. Li, S. Mu, *Angew. Chem. Int. Ed.* **2017**, *56*, 11559-11564.

[94] T. Liu, S. Wang, Q. Zhang, L. Chen, W. Hu, C. M. Li, *Chem. Commun.* **2018**, *54*, 3343-3346.

[95] T. Liu, B. Feng, X. Wu, Y. Niu, W. Hu, C. M. Li, *ACS Appl. Energy Mater.* **2018**, *1*, 3143-3150.

[96] T. Cheng, L. Wang, B. V. Merinov, W. A. Godard III, *J. Am. Chem. Soc.* **2018**, *140*, 7787-7790.

[97] J. Yu, Y. Guo, S. She, S. Miao, M. Ni, W. Zhou, M. Liu, Z. Shao, *Adv. Mater.* **2018**, *30*, 1800047.

[98] J. Liu, Y. Zheng, D. Zhu, A. Vasileff, T. Ling, S.-Z. Qiao, *Nanoscale* **2017**, *9*, 16616-16621.

[99] P. Jiang, Y. Yang, R. Shi, G. Xia, J. Chen, J. Su, Q. Chen, *J. Mater. Chem. A* **2017**, *5*, 5475-5485.

[100] E. Demir, S. Akbayrak, A. M. Önal, S. Özkar, *J. Colloid Interface Sci.* **2018**, *531*, 570-577.

[101] U. Joshi, S. Malkhandi, Y. Ren, T. L. Tan, S. Y. Chiam, B. S. Yeo, *ACS Appl. Mater. Interfaces* **2018**, *10*, 6354-6360.

[102] L. Zhu, Q. Cai, F. Liao, M. Shengb, B. Wub, M. Shao, *Electrochem. Commun.* **2015**, *52*, 29-33.

[103] X. Yang, Z. Zhao, X. Yu, L. Feng, *Chem. Commun.* DOI: 10.1039/c8cc09993f.

[104] Y. Liu, X. Lu, Z. Che, C. Zhang, M. Han, J. Bao, Z. Dai, *Chem. Commun.* **2018**, *54*,12202-12205.

[105] E. Demir, S. Akbayrak, A. M. Önal, S. Özkar, *ACS Appl. Mater. Interfaces* **2018**, *10*, 6299-6308.

[106] J. Su, Y. Yang, G. Xia, J. Chen, P. Jiang, Q. Chen, *Nat. Commun.* **2017**, *8*, 14969.

[107] Y. Xu, Y. Li, S. Yin, H. Yu, H. Xue, X. Li, H. Wang, L. Wang, *Nanotechnology* **2018**, *29*, 225403.

[108] S. Liu, Q. Liu, Y. Lv, B. Chen, Q. Zhou, L. Wang, Q. Zheng, C. Che, C. Chen, *Chem. Commun.* **2017**, *53*, 13153-13156.

[109] Y. Liu, S. Liu, Y. Wang, Q. Zhang, L. Gu, S. Zhao, D. Xu, Y. Li, J. Bao, Z. Dai, *J. Am. Chem. Soc.* **2018**, *140*, 2731-2734.

[110] R. K. Shervedani, M. Torabi, M. S. Foroushani, *J. Phys. Chem. C* **2018**, *122*, 17621-17631.

[111] Y. Yamada, S. Shikano, S. Fukuzumi, *J. Phys. Chem. C* **2013**, *117*, 13143-13152.

[112] Y. Yamada, T. Miyahigashi, H. Kotani, K. Okubo, S. Fukuzumi, *J. Am. Chem. Soc.* **2011**, *133*, 16136-16145.

[113] S. Fukuzumi, Y. Yamada, *J. Mater. Chem.* **2012**, *22*, 24284-24296.

[114] Y. Yamada, T. Miyahigashi, K. Ohkubo, S. Fukuzumi, *Phys. Chem. Chem. Phys.* **2012**, *14*, 10564-10571.

[115] C. Kong, Z. Li, G. Lu, *Int. J. Hydrogen Energy* **2015**, *40*, 5824-5830.

[116] Y. Yamada, K. Yano, S. Fukuzumi, *Aust. J. Chem.* **2012**, *65*, 1573-1581.

[117] L. Francàs, E. Burns, L. Steier, H. Cha, L. Solà, X. Li, P. Shakya, R. Bofill, J. García-Antón, X. Sala, J. R. Durrant. *Chem. Commun*. **2018**, 54, 5732-5735.

[118] M. A. Melo, Jr., Z. Wu, B. A. Nail, A. T. De Denko, A. F. Nogueira, F. E. Osterloh, *Nano Lett.* **2018**, *18*, 805-810.

[119] Q. Wang, T. Hisatomi, Q. Jia, H. Tokudome, M. Zhong, C. Wang, Z. Pan, T. Takata, M. Nakabayashi, N. Shibata, Y. Li, I. D. Sharp, A. Kudo, T. Yamada, K. Domen, *Nat. Mater.* **2016**, *15*, 611-615.